

國立交通大學

電信工程研究所

碩士論文

應用於單頻段和多頻段之新型印刷式天線
之設計及量測



Three Novel Printed Antennas for Single- and
Multiple-Band Applications

研究生：陳凱得

指導教授：鍾世忠 博士

中華民國九十三年六月

Three Novel Printed Antennas for Single- and Multiple-Band Applications

研究生：陳凱得

Student: Kai-Te Chen

指導教授：鍾世忠 博士

Advisor: Dr. Shyh-Jong Chung

國立交通大學

電信工程研究所

碩士論文



Submitted to Institute of Communication

College Electrical Engineering and Computer Science

National Chiao Tung University

In Partial Fulfillment of the Requirements

for the Degree of Master of Science

In Communication Engineering

June 2004

中華民國九十三年六月

應用於單頻段與多頻段之新型印刷式天線之設計與量測

研 究 生：陳凱得

指導教授：鍾世忠 博士

國立交通大學 電信工程學系碩士班

摘要

這篇論文中展示了三隻新型的印刷式天線。首先介紹一支 2.4 GHz 的印刷式倒 E 型天線，它是一種改良的印刷式倒 F 天線，利用在開路支線端增加一個類似平行板電容的電容性負載來縮小天線的尺寸，而它的幅射場型相當於全向性，最大的天線增益有 2.09 dBi。接著介紹一支工作在 2.4 GHz 和 5 GHz 的雙頻天線，利用一個微帶線抗流器使電流在高頻時無法進入調整的金屬線中，而達到雙頻的效果，它在低頻的幅射場型相當於一般印刷式單極天線的場型，而在高頻則是接近全向性的場型，最大的天線增益在低頻有 2.43 dBi 而在高頻有 4.58 dBi。最後再利用相似的原理設計一個工作在 0.9 GHz、1.8 GHz、1.9 GHz 和 2.4 GHz 的多頻天線，可做為 GSM 和 WLAM 應用整合的天線。

Three Novel Printed Antenna for Single- and Multiple- Applications

Student: Kai-Te Chen

Advisor: Dr. Shyh-Jong Chung

Institute of Communication engineering

National Chiao Tung University

ABSTRACT

Three novel printed antennas for single- and multiple-band applications are exhibited in this thesis. First, we will show a printed inverted-E antenna which is modified from a printed inverted-F antenna but with a printed capacitance load to reduce the antenna size. It has an omni-directional radiation pattern with a maximum gain of 2.09 dBi. Then, we show a dual-band antenna with a microstrip choke for 2.4 GHz and 5 GHz applications. The microstrip choke prevents the current at higher band entering the tuning metal line. Its radiation patterns at lower band are like a printed monopole antenna and are omni-directional at higher band. The maximum gain is 2.43 dBi for lower band and 4.58 dBi for higher band. Finally, we utilize similar principle to design a multiple-band antenna at 0.9 GHz, 1.8 GHz, 1.9 GHz and 2.4 GHz. It is suitable for GSM and WLAN integration applications.

Acknowledgement

本篇論文能夠順利的完成，首先要特別感謝我的指導教授 鍾世忠老師，不僅提供了相當好且資源充足的一個研究環境，讓我在學習的路上無後顧之憂；而且在我遇到困難、瓶頸時，都能給予我正確的方向進而修正許多迷思的觀念，老師在天線應用上豐富以及深厚的學識，的確像是一座大寶藏，挖也挖不完、學也學不完。另外，老師待人寬厚、親切與學生互動良好的態度，兩年之中也一直是 我待人處世的模範。再來也要感謝口試委員蔡文濬博士、郭仁財老師和林怡成老師撥冗對我的論文提出一些建議，使得論文內容能更完備。此外，要再謝謝中華電信的劉威廷學長以及工研院的周天祺學長，在 GSM 900/1800/1900 頻段天線遠場的量測上的幫忙，才能讓論文順利完成。

接著要謝謝兩年來一直陪伴著我走過來的實驗室同學們，謝謝小雅（雅瑩）、小洲洲（明洲）、伸憶、怡力在天線設計領域上經驗的分享以及互相討論所激發出創新的想法；謝謝全哥（信全）、揚裕、俊甫對我的在微波工程、微波電路上的問題都能不厭其煩幫我解答。並謝謝博士班何丹雄同學、碩一學弟妹：侑信、清文、民仲、珮如、實驗室助理又正以及碩二的全體同學，一起渡過兩年美好的時光。

最後要謝謝我的父母，從小辛苦的養育我，即使唸到了研究所，也能讓我在沒經濟的壓力下成長，並且讓我有自主的空間，但在我迷惘的時候，又能適時拉我一把，也謝謝弟弟妹妹，讓我隨時都能感受到親情的溫暖。當然也要謝謝我的女朋友珮茹，在這兩年來能夠包容我忙碌的生活以及一同分享我的喜怒哀樂，另外還要謝謝虹韻土風舞社的全體社員，特別是同屆的為昱、家輝、彥易、柏瑄、心怡，陪我渡過休閒時的歡樂時光，讓我的研究壓力都能獲得舒解。

要謝謝的人實在太多了，僅以這篇論文獻給所有關心我的人。

Content

摘要.....	I
ABSTRACT.....	II
ACKNOWLEDGEMENT.....	III
CONTENT.....	IV
TABLE LIST.....	VI
FIGURE LIST.....	VIII
CHAPTER 1: INTRODUCTION.....	1-1
1.1 BACKGROUND AND MOTIVATION	1-1
1.2 ORGANIZATION	1-3
CHAPTER 2: THEORY OF PRINTED ANTENNAS	2-1
2.1 DIPOLE ANTENNAS.....	2-1
2.2 MONOPOLE ANTENNAS	2-2
2.3 INVERTED-L ANTENNAS	2-2
2.4 PRINTED ANTENNAS.....	2-3
2.5 PRINTED INVERTED-F ANTENNAS	2-6
CHAPTER 3: DESIGN AND MEASUREMENT OF THE PRINTED	
INVERTED-E ANTENNA	3-1
3.1 DESIGN THEORY.....	3-1
3.2 SIMULATED AND MEASURED RESULTS	3-2
3.3 ANALYSIS	3-4

CHAPTER 4: DESIGN AND MEASUREMENT OF A DUAL-BAND

MONOPOLE ANTENNA WITH A MICROSTRIP CHOKE4-1

4.1 DESIGN THEORY4-1

4.2 SIMULATED AND MEASURED RESULTS4-2

4.3 ANALYSIS4-7

CHAPTER 5: DESIGN AND MEASUREMENT OF A MULTIPLE-BAND

MONOPOLE ANTENNA WITH A MICROSTRIP CHOKE5-1

5.1 DESIGN THEORY5-1

5.2 SIMULATED AND MEASURED RESULTS5-1

5.3 ANALYSIS5-4

CHAPTER 6: CONCLUSIONS6-1

REFERENCE..... A

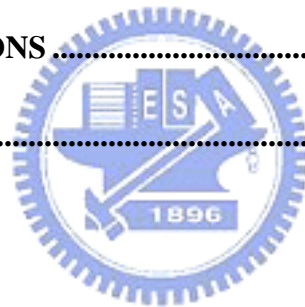


Table List

TABLE 1-1: THREE GSM BAND	1-1
TABLE 3-1: THE MAXIMUM AND AVERAGE GAIN OF THE PRINTED INVERTED-E ANTENNA IN THE X-Z, Y-Z AND X-Y PLANE AT 2.44 GHz.	3-2
TABLE 3-2: THE MAXIMUM AND AVERAGE GAIN OF THE PRINTED INVERTED-E ANTENNA WITH A CASE IN THE X-Z, Y-Z AND X-Y PLANE AT 5.77 GHz.	3-3
TABLE 4-1: THE MAXIMUM AND AVERAGE GAIN OF THE DUAL-BAND ANTENNA IN THE X-Z, Y-Z AND X-Y PLANE AT 2.44 GHz.	4-3
TABLE 4-2: THE MAXIMUM AND AVERAGE GAIN OF THE TYPICAL MONOPOLE ANTENNA IN THE X-Z, Y-Z AND X-Y PLANE AT 2.44 GHz.	4-3
TABLE 4-3: THE MAXIMUM AND AVERAGE GAIN OF THE DUAL-BAND ANTENNA IN THE X-Z, Y-Z AND X-Y PLANE AT 5.25 GHz.	4-4
TABLE 4-4: THE MAXIMUM AND AVERAGE GAIN OF THE DUAL-BAND ANTENNA IN THE X-Z, Y-Z AND X-Y PLANE AT 5.77 GHz.	4-4
TABLE 4-5: THE MAXIMUM AND AVERAGE GAIN OF THE MODIFIED DUAL-BAND ANTENNA IN THE X-Z, Y-Z AND X-Y PLANE AT 2.44 GHz.	4-6
TABLE 4-6: THE MAXIMUM AND AVERAGE GAIN OF THE MODIFIED DUAL-BAND ANTENNA IN THE X-Z, Y-Z AND X-Y PLANE AT 5.25 GHz.	4-6
TABLE 4-7: THE MAXIMUM AND AVERAGE GAIN OF THE MODIFIED DUAL-BAND ANTENNA IN THE X-Z, Y-Z AND X-Y PLANE AT 5.77 GHz.	4-7
TABLE 5-1: THE MAXIMUM AND AVERAGE GAIN OF THE MULTIPLE-BAND ANTENNA IN THE X-Z, Y-Z AND X-Y PLANE AT 0.92 GHz.	5-2
TABLE 5-2: THE MAXIMUM AND AVERAGE GAIN OF THE MULTIPLE-BAND ANTENNA IN THE X-Z, Y-Z AND X-Y PLANE AT 1.795 GHz.	5-3

TABLE 5-3: THE MAXIMUM AND AVERAGE GAIN OF THE MULTIPLE-BAND ANTENNA IN
THE X-Z, Y-Z AND X-Y PLANE AT 1.92 GHz.5-3

TABLE 5-4: THE MAXIMUM AND AVERAGE GAIN OF THE MULTIPLE-BAND ANTENNA IN
THE X-Z, Y-Z AND X-Y PLANE AT 2.44 GHz.5-4



Figure List

FIGURE 2-1: CURRENT DISTRIBUTION AND RADIATION PATTERN OF THE HALF-WAVE DIPOLE	2-8
FIGURE 2-2: MONOPOLE ANTENNA FED AGAINST A GROUND PLANE WITH A COAXIAL CABLE	2-9
FIGURE 2-3: TRANSMISSION LINE LOADED ANTENNA	2-9
FIGURE 2-4: THE INVERTED-L ANTENNA	2-10
FIGURE 2-5: PRINTED TRANSMISSION LINES	2-10
FIGURE 2-6: QUASI-TEM APPROXIMATION	2-10
FIGURE 2-7: TWO KINDS OF PRINTED ANTENNAS	2-11
FIGURE 2-8: IMPEDANCE VARIATION ALONG A TRANSMISSION LINE	2-11
FIGURE 2-9: EQUIVALENT MODEL OF THE PRINTED INVERTED-F ANTENNA	2-12
FIGURE 3-1: GEOMETRY OF THE PRINTED INVERTED-E ANTENNA	3-6
FIGURE 3-2: EQUIVALENT CAPACITANCE OF THE DECREASED LENGTH EQUALS THE CAPACITIVE LOAD	3-7
FIGURE 3-3: PHOTOGRAPHY OF THE PRINTED INVERTED-E ANTENNA	3-7
FIGURE 3-4: SIMULATED AND MEASURED RETURN LOSS OF THE PRINTED INVERTED-E ANTENNA	3-8
FIGURE 3-5: CURRENT DENSITY DISTRIBUTION OF THE INVERTED-E ANTENNA	3-8
FIGURE 3-6: MEASURED RADIATION PATTERNS OF THE PRINTED INVERTED-E ANTENNA AT 2.44 GHz	3-9
FIGURE 3-7: PHOTOGRAPHY OF THE PRINTED INVERTED-E ANTENNA WITH A CASE ...	3-10
FIGURE 3-8: SIMULATED AND MEASURED RETURN LOSS OF THE PRINTED INVERTED-E ANTENNA WITH A CASE	3-10

FIGURE 3-9: MEASURED RADIATION PATTERNS OF THE PRINTED INVERTED-E ANTENNA WITH A CASE AT 2.44 GHz	3-11
FIGURE 3-10: MEASURED GAIN OF THE PRINTED INVERTED-E ANTENNA VERSUS FREQUENCY	3-12
FIGURE 3-11: SIMULATED RETURN LOSS VERSUS FREQUENCY FOR DIFFERENT H_C	3-12
FIGURE 3-12: EQUIVALENT CIRCUIT MODEL OF THE PRINTED INVERTED-E ANTENNA WITHOUT THE CAPACITIVE LOAD	3-13
FIGURE 3-13: RETURN LOSS OF THE EQUIVALENT CIRCUIT IN FIGURE 3-12	3-13
FIGURE 3-14: EQUIVALENT CIRCUIT OF THE PRINTED INVERTED-E ANTENNA	3-14
FIGURE 3-15: RETURN LOSS OF THE EQUIVALENT CIRCUIT IN FIGURE 3-14	3-14
FIGURE 3-16: RETURN LOSS OF THE PRINTED INVERTED-E AND INVERTED-F ANTENNA AT THE SAME RESONANT FREQUENCY	3-15
FIGURE 4-1: SCHEMATIC DIAGRAM OF THE DUAL-BAND ANTENNA.....	4-9
FIGURE 4-2: GEOMETRY OF THE DUAL-BAND ANTENNA	4-9
FIGURE 4-3: PHOTOGRAPHY OF THE DUAL-BAND ANTENNA	4-10
FIGURE 4-4: MEASURED AND SIMULATED RETURN LOSS OF THE DUAL-BAND ANTENNA	4-10
FIGURE 4-5: CURRENT DENSITY DISTRIBUTION OF THE DUAL-BAND ANTENNA.....	4-11
FIGURE 4-6: DUAL-BAND ANTENNA COMPARED WITH THE TYPICAL MONOPOLE ANTENNA	4-11
FIGURE 4-7: MEASURED RADIATION PATTERNS OF THE DUAL-ANTENNA AT 2.44 GHz	4-12
FIGURE 4-8: MEASURED RADIATION PATTERNS OF THE TYPICAL MONOPOLE ANTENNA AT 2.44 GHz.....	4-13
FIGURE 4-9: MEASURED RADIATION PATTERNS OF THE DUAL-ANTENNA AT 5.25 GHz	4-14

FIGURE 4-10: MEASURED RADIATION PATTERNS OF THE DUAL-ANTENNA AT 5.77 GHz	4-15
.....	4-15
FIGURE 4-11: PHOTOGRAPHY OF THE MODIFIED DUAL-BAND ANTENNA	4-16
FIGURE 4-12: SIMULATED AND MEASURED RETURN LOSS OF THE MODIFIED DUAL-BAND ANTENNA	4-16
.....	4-16
FIGURE 4-13: MEASURED RADIATION PATTERNS OF THE MODIFIED DUAL-ANTENNA AT 2.44 GHz	4-17
.....	4-17
FIGURE 4-15: MEASURED RADIATION PATTERNS OF THE MODIFIED DUAL-ANTENNA AT 5.25 GHz	4-18
.....	4-18
FIGURE 4-16: MEASURED RADIATION PATTERNS OF THE DUAL-ANTENNA AT 5.77 GHz	4-19
.....	4-19
FIGURE 4-17: DESIGN FLOW OF THE DUAL-BAND ANTENNA	4-20
FIGURE 4-18: THE RESULT OF THE DUAL-BAND ANTENNA FROM DESIGN FLOW	4-20
FIGURE 4-19: SEVERAL KINDS OF THE CHOKE SHAPE	4-21
FIGURE 4-20: SIMULATED RETURN LOSS OF THE DUAL-BAND ANTENNA WITH DIFFERENT CHOKE	4-21
.....	4-21
FIGURE 4-21: SIMULATED RETURN LOSS OF THE DUAL-BAND ANTENNA WITH DIFFERENT TUNING METAL LINE LENGTH	4-22
.....	4-22
FIGURE 5-1: PHOTOGRAPHY OF THE MULTIPLE-BAND ANTENNA	5-5
FIGURE 5-2: SIMULATED AND MEASURED RETURN LOSS OF THE MULTIPLE-BAND ANTENNA	5-5
.....	5-5
FIGURE 5-3: CURRENT DISTRIBUTION OF THE MULTIPLE-BAND ANTENNA AT 0.9 GHz BAND	5-6
.....	5-6
FIGURE 5-4: CURRENT DISTRIBUTION OF THE MULTIPLE-BAND ANTENNA AT 1.8 GHz BAND	5-6
.....	5-6
FIGURE 5-5: CURRENT DISTRIBUTION OF THE MULTIPLE-BAND ANTENNA AT 1.9 GHz	

BAND.....5-7

FIGURE 5-6: CURRENT DISTRIBUTION OF THE MULTIPLE-BAND ANTENNA AT 2.4 GHZ

BAND.....5-7

FIGURE 5-7: RADIATION PATTERNS OF THE MULTIPLE-BAND ANTENNA AT 0.92 GHZ...5-8

FIGURE 5-8: RADIATION PATTERNS OF THE MULTIPLE-BAND ANTENNA AT 1.795 GHZ.5-9

FIGURE 5-9: RADIATION PATTERNS OF THE MULTIPLE-BAND ANTENNA AT 1.92 GHZ.5-10

FIGURE 5-10: RADIATION PATTERNS OF THE MULTIPLE-BAND ANTENNA AT 2.44 GHZ5-11

FIGURE 5-11: RESULT OF THE DUAL-BAND ANTENNA SECTION FROM THE DESIGN FLOW

.....5-12

FIGURE 5-12: COMPARISON WITH EACH SECTION OF THE MULTIPLE-BAND ANTENNA 5-12




Chapter 1: Introduction

1.1 Background and Motivation

Wireless communications have enormous growth in the last decade. The Global System for Mobile communications (GSM) and the Wireless Local Area Networks (WLAN) are two of the most important systems today. The GSM system was specified by the European Telecommunications Standards Institute (ETSI) and has rapidly gained acceptance and market share worldwide. The WLAN provides a viable extension of wired LAN for various business applications.

In principle the GSM system can be implemented in any frequency band. However there are several bands where GSM terminals are available and list above:



GSM 900	880 - 915 MHz paired with 925 - 960 MHz
GSM 1800	1710 - 1785 MHz paired with 1805 - 1880 MHz
GSM 1900	1850 - 1910 MHz paired with 1930 - 1990 MHz

Table1-1: Three GSM band

In the above bands mobile stations transmit in the lower frequency sub-band and base stations transmit in the higher frequency sub-band. Furthermore, GSM terminals may incorporate one or more of the GSM frequency bands listed above to facilitate roaming on a global basis.

All of the WLAN standards have been developed by the Institute of Electrical and Electronics Engineers (IEEE). 802.11 is a family of specifications developed by the IEEE for wireless LAN technology. 802.11 specifies an over-the-air interface between a wireless client and a base station. 802.11 is broken down into three

principal sub-levels; 802.11a, 802.11b, and lastly 802.11g. These 802.11 sub standards are all very similar in basic theory and the only major differences are in rate at which the data is transferred and the frequency bands in which they operate.

Probably 802.11b is considered to be the most common standard when dealing with home and small business WLAN and is also regarded as the standard that started it all when referring to wireless networking. 802.11b is the original bearer of the “Wi-Fi” (short for Wireless Fidelity) name, which it was given in 1999 to avoid sounding too techie. 802.11b operates in 2.4 GHz to 2.4835 GHz frequency band over eleven available frequency channels in U.S. at transfer rates up to 11 Mbps within 100 feet of the wireless access point (WAP). The speed will drop off significantly as the user moves away from the WAP to the point that the speed will be as low as 1 Mbps at 300 feet away.

802.11a is the second generation standard of wireless networking to have been introduced. This standard is much faster, nearly 5 times faster, than its predecessor 802.11b operating in 5.15 GHz to 5.35 GHz and 5.725GHz to 5.825 GHz frequency band over eight available frequency channels in U.S. at transfer rates up to 54 Mbps. 802.11a and 802.11b are not compatible as they both operate in different frequency ranges and this is not to 802.11a's advantage as the majority of WLAN equipment sold to date has been for 802.11b. The maximum operating range of 150 feet for 802.11a is shorter than the maximum of 300 feet for 802.11b.

The third generation standard 802.11g is a combination of both 802.11b and 802.11a. Much like its predecessor 802.11b, 802.11g operates in the 2.4 GHz range over the eleven available in the U.S. The 802.11g transfer rates, however, take after 802.11a and are in the speed range up around 54 Mbps and can transmit up to nearly 1500 feet if the signal is unobstructed. 802.11g is backward compatible with 802.11b, but not 802.11a. Backward compatible means that 802.11g wireless access cards can be used to connect to WLANs

using 11b WAPs, but not vice-versa. Often thought of as the best alternative between faster 802.11a and the older and slower 802.11b, 802.11g is likely to make the most sense for consumers and small businesses in the future [1].

The antenna is one of the most important devices in the front end of wireless communications. However, the antenna size is often much larger than other circuits in the system. How to reduce the antenna size or achieve dual-band operation are targets that many scientists and engineers pursue. Several researches about the miniature and dual-band antennas for GSM and 802.11 a/b/g applications are shown in many scientific or technical literatures [2] - [14]. We will exhibit three antennas including a compact antenna, a dual-band antenna and a multiple-band antenna.

1.2 Organization

This thesis is devoted to the three novel printed antennas for single- and multiple-band applications. It consists of six chapters. Chapter 1 gives the introduction of wireless communication and the development of the printed antennas.

In chapter 2, we will deal with the design methodology of the printed antennas. The typical dipole, monopole, the inverted-L antennas and the printed antennas characteristics are described; in the meantime, the printed inverted-F antennas are also discussed.

Chapter 3 exhibits the printed inverted-E antennas utilizing a parallel plate capacitive load to reduce the antenna size. The influence of adding a case to the antenna is also specified. Last of all, both the simulated and measured results will be brought to comparison.

In chapter 4, the design of the dual-band antenna with a microstrip choke will be introduced. A modified dual-band antenna is also shown for reducing the dual-band antenna size. Last of all, both the simulated and measured results will be brought to

comparison

Chapter 5 presents the multiple-band antenna with a microstrip choke. Both the simulated and measured results will be brought to comparison.

Chapter 6 will combine the summary and indicates some suggestions for the printed antennas design in the future.



Chapter 2: Theory of Printed Antennas

The categories of antennas in this thesis are all printed antennas including modified printed monopole antennas and modified printed inverted-F antennas. Hence we will introduce some basic theories about printed antennas in this chapter first.

2.1 Dipole Antennas

Dipole antennas have three basic types: the ideal, short and half-wave dipoles. The ideal and short dipoles have uniform and triangular current distributions, respectively. The half-wave dipoles that are widely used have a linear current whose amplitude varies as one-half of a sine wave with a maximum at the center. The advantage of a half-wave dipole is that it can be made to resonate and present a zero input reactance, thus eliminating the need for tuning to achieve a conjugate impedance match. The input impedance of an infinitely thin half-wavelength dipole is $73 + j42.5\Omega$. If it is slightly reduced in length to achieve resonance, the input impedance is about $70 + j0\Omega$. Therefore, if we want to obtain a resonant condition for a half-dipole, the physical length must be a bit shorter than a half-wavelength of the electromagnetic wave propagating in the free space, and as the antenna width is increased, the length must be reduced more to achieve resonance.

As usual, the current distribution is placed along the z -axis and for the half-sine wave current on the half-wave dipole, the current distribution is written as

$$I(z) = I_m \sin\left[\mathbf{b}\left(\frac{l}{4} - |z|\right)\right], \quad |z| \leq \frac{l}{4} \quad (2-1)$$

where $\mathbf{b} = 2\mathbf{p}/l$. This current goes to zero at the ends (for $z = \pm l/4$) and its maximum value I_m occurs at the center ($z = 0$) as shown in Fig. 2-1a. From this current distribution, we can calculate the radiation pattern by antenna theory [15]. So

we can obtain the complete far-field radiation pattern is

$$F(\mathbf{q}) = g(\mathbf{q})f(\mathbf{q}) = \sin \mathbf{q} \frac{\cos[(\mathbf{p}/2)\cos \mathbf{q}]}{\sin^2 \mathbf{q}} = \frac{\cos[(\mathbf{p}/2)\cos \mathbf{q}]}{\sin \mathbf{q}} \quad (2-2)$$

where $g(\mathbf{q})$ is the element factor and $f(\mathbf{q})$ is the normalized radiation pattern factor. This pattern is plotted in Fig. 2-2b in polar form with linear scale.

2.2 Monopole Antennas

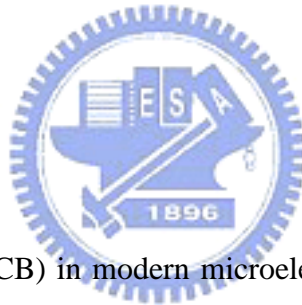
The monopole antennas are the dipole antennas that have been divided in half at its center feed point and fed against a ground plane, as shown in Fig. 2-2 (a). In practice, the monopole antennas have more widespread applications than the dipole antennas since the antennas must integrate with other circuits on a reference ground plane. From the image theory [15], the current and charges on a monopole are the same as on the upper half of its dipole counterpart, as shown in Figure 2-2 (b). But the terminal voltage is only half that of the dipole because the gap width of the input terminal is half that of the dipole. Therefore, the input impedance for a monopole is therefore half that of its dipole counterpart and the input impedance of an infinitesimally thin quarter-wave monopole is $(72 + j42.5)/2 = 36 + j21.3 \Omega$. The radiation pattern of the monopole antennas is similar to the one of the dipole antennas.

2.3 Inverted-L Antennas

To reduce the antenna size, the inverted-L antennas is a good choice. Inverted-L antennas can take as transmission line loaded antennas fed against an infinite large ground plane. Transmission line loaded antennas are small antennas which used to approximate the ideal dipole antennas, as shown in Figure 2-3 (a). The results of transmission line theory can be borrowed to determine the current. The current is essentially sinusoidal along the wire with a zero at the ends. This current distribution

is sketched in Figure 2-3 (b) for $L < \lambda/4$. If $\Delta z \ll \lambda$, the field from the currents on the horizontal wires essentially cancel in the far field. If also $\Delta z \ll L$, the horizontal wires provide an effective place for the charge to be stored and the current on the vertical section is nearly constant as illustrated in Figure 2-3 (b). Then radiation comes from a short section over which the current is nearly constant and the antenna approximates an ideal dipole. Transmission line loading ideas can be extended by attaching several horizontal wires to the ends of the short vertical section. As more wires are added, the reactance is further reduced. From the image theory, the monopoles form of the transmission line loaded dipole shown in Figure 2-4 are called the inverted-L antennas. Similar to the transmission loaded antennas, the inverted-L antennas radiate mainly by the vertical section and the horizontal section is mainly for impedance matching.

2.4 Printed Antennas



Printed circuit boards (PCB) in modern microelectronics industry is widespread used to design for several applications. The use of printed circuits reduces the size and normalizes the designs. The transmission line used on the PCB is microstrip line or coplanar waveguide (CPW) as shown in Figure 2-5. Using microstrip line or CPW is easily integrated with other passive and active microwave device. The fields in a real microstrip line extend within two media, air above and dielectric below, so that the structure is inhomogeneous. For a transverse electromagnetic (TEM) wave, the propagation velocity depends only on the material properties ϵ and μ . Within two materials, TEM waves propagate with two velocities, one within the other in the air above the interface. Assume the conductor thickness is infinitely thin; the boundary conditions on the interface require the continuity of the tangential components and cannot be satisfied. As a result, the propagation along a microstrip line cannot be pure

TEM. If we consider the Maxwell's equations and boundary conditions, it was shown that the longitudinal components of the electric and of the magnetic field of the dominant mode do not vanish but the longitudinal components of the fields for the dominant mode remain very much smaller than the transverse components and may therefore be neglected. The dominant mode then behaves like a TEM mode and the homogeneous uniform line remain valid for its analysis. So this is called the quasi-TEM approximation.

In the quasi-TEM approximation, the inhomogeneous microstrip line is replaced by a homogeneous structure, in which the conductors retain the same geometry (w, h, t) but are immersed in a single dielectric of effective permittivity ϵ_e as shown in Figure 2-6.

The low-frequency value of ϵ_e is determined by evaluating the capacitance of the inhomogeneous structure, yielding approximate relationship

$$\epsilon_e \cong \frac{\epsilon_r + 1}{2} + \frac{\epsilon_r - 1}{2} \left(1 + 10 \frac{h}{w}\right)^{-ab} \quad (2-3)$$

with

$$a = 1 + \frac{1}{49} \log \frac{(w/h)^4 + (w/52h)^2}{(w/h)^4 + 0.432} + \frac{1}{18.7} \log \left\{1 + \left(\frac{1}{18.1} \frac{w}{h}\right)^3\right\}$$

$$b = 0.564 \left(\frac{\epsilon_r - 0.9}{\epsilon_r + 3}\right)^{0.053}$$

The accuracy provided by this approximation is better than 0.2% for $0.01 \leq w/h \leq 100$ and $1 \leq \epsilon_r \leq 128$ [16]. Generally, we reduce above relationship to a simpler form [17]

$$\epsilon_e \cong \frac{\epsilon_r + 1}{2} + \frac{\epsilon_r - 1}{2} \frac{1}{\sqrt{1 + 12h/w}} \quad (2-4)$$

Given the dimensions of the microstrip line, the characteristic impedance can be

calculated as

$$Z_0 = \begin{cases} \frac{60}{\sqrt{\epsilon_e}} \ln\left(\frac{8h}{w} + \frac{w}{4h}\right) & \text{for } w/h \leq 1 \\ \frac{120\mathbf{p}}{\sqrt{\epsilon_e} [w/h + 1.393 + 0.667 \ln(w/h + 1.444)]} & \text{for } w/h \geq 1 \end{cases} \quad (2-5)$$

For a given characteristic impedance Z_0 and dielectric constant ϵ_r , the w/h ratio can be found as

$$\frac{w}{h} = \begin{cases} \frac{8e^A}{e^{2A} - 2} & \text{for } w/h < 2 \\ \frac{2}{\mathbf{p}} [B - 1 - \ln(2B - 1) + \frac{\epsilon_r - 1}{2\epsilon_r} \{ \ln(B - 1) + 0.39 - \frac{0.61}{\epsilon_r} \}] & \text{for } w/h > 2 \end{cases} \quad (2-6)$$

where

$$A = \frac{Z_0}{60} \sqrt{\frac{\epsilon_r + 1}{2} + \frac{\epsilon_r - 1}{\epsilon_r + 1}} \left(0.23 + \frac{0.11}{\epsilon_r}\right)$$

$$B = \frac{377\mathbf{p}}{2Z_0\sqrt{\epsilon_r}}$$

From above microstrip line model, we can know the physical length of a printed antenna is shorter than the one of a wire antenna. And since it is convenient to integrate with other circuits in the front end and is easy to manufacture, printed antennas are extensively used. Generally, the printed monopole antennas and the printed inverted-F antennas are two of the printed antennas that engineers use most often on the PCB. The structure of the two antennas is as shown in Figure 2-7. The dash line indicates the ground plane region. To effectively use the area on the PCB, the printed monopole antenna usually places in a side area which has no ground metal but two sides of the region are adjacent to ground planes. So the printed monopole antenna has two image ground planes in the region. The two image ground planes all can influence the radiation characteristics of the printed monopole antenna. The

printed inverted-F antennas save more areas than printed monopole antennas because of their lateral structures. We will discuss the principle of the printed inverted-F antennas in next section.

2.5 Printed inverted-F antennas

The structure of the printed inverted-F antenna is shown in Figure 2-7 (b). The principle of the printed inverted-F antennas is similar to the planar inverted-F antennas (PIFA). But the printed antennas have simpler structures and manufacture process than the PIFA. From the transmission line theory [17], the input impedance Z_{in} of a length l of the transmission line with arbitrary load impedance Z_L is

$$Z_{in} = Z_0 \frac{Z_L + jZ_0 \tan \mathbf{b}l}{Z_0 + jZ_L \tan \mathbf{b}l} \quad (2-7)$$

where Z_0 and \mathbf{b} are the characteristic impedance and phase constant of the transmission line. When the load is short-circuited, the input impedance equals

$$Z_{in} = jZ_0 \tan \mathbf{b}l \quad (2-8)$$

and when the load is open-circuited, the input impedance equals

$$Z_{in} = -jZ_0 \cot \mathbf{b}l \quad (2-9)$$

Figure 2-8 shows the impedance variation along a short-circuited and an open-circuited transmission line. We can find if the length l of the transmission line is shorter than $\lambda/4$, the short-circuited transmission line is inductive and the open-circuited one is capacitive. Hence, if the length from the short point to the open end equals $\lambda/4$, printed inverted-F antenna looks like a short-circuited transmission line shunt with an open-circuited transmission line and the two transmission lines are both shorter than $\lambda/4$. Now, the antenna which is composed of the two transmission

lines is like a RLC resonator so that let the antenna resonate to radiate. The equivalent model is shown in Figure 2-9. The $G_r = 1/R_r$ in Figure 2-9 is the radiation conductance. So the input admittance at the feed point is

$$Y_{in} = -jY_0 \cot \mathbf{b}l_1 + Y_0 \frac{G_r + jY_0 \tan \mathbf{b}l_2}{Y_0 + jG_r \tan \mathbf{b}l_2} \quad (2-10)$$

and $l_1 + l_2 = \mathbf{l} / 4$,

$$\cot \mathbf{b}l_1 = \cot \mathbf{b}(\mathbf{l} / 4 - l_2) = \cot(\mathbf{p} / 2 - \mathbf{b}l_2) = \tan \mathbf{b}l_2 \quad (2-11)$$

Substitution of (2-11) into (2-10) gives

$$\begin{aligned} Y_{in} &= -jY_0 \tan \mathbf{b}l_2 + Y_0 \frac{G_r + jY_0 \tan \mathbf{b}l_2}{Y_0 + jG_r \tan \mathbf{b}l_2} \\ &= \frac{-jY_0^2 \tan \mathbf{b}l_2 + Y_0 G_r \tan^2 \mathbf{b}l_2 + Y_0 G_r + jY_0^2 \tan \mathbf{b}l_2}{Y_0 + jG_r \tan \mathbf{b}l_2} \\ &\cong \frac{Y_0 G_r \tan^2 \mathbf{b}l_2 + Y_0 G_r}{Y_0} \\ &\cong G_r \sec^2 \mathbf{b}l_2 \end{aligned} \quad (2-12)$$

The result of (2-12) is a real number so that the antenna resonates as to radiate. From Figure 2-9 we also can obtain

$$j\omega L_F = jZ_0 \tan \mathbf{b}l_1 \quad (2-13)$$

and

$$j\omega C_F = jY_0 \tan \mathbf{b}l_2 \quad (2-14)$$

We multiply (2-13) and (2-14) together,

$$\begin{aligned} \omega^2 L_F C_F &= \tan \mathbf{b}l_1 \tan \mathbf{b}l_2 \\ &= \tan \mathbf{b}(\mathbf{l} / 4 - l_2) \tan \mathbf{b}l_2 \\ &= \cot \mathbf{b}l_2 \tan \mathbf{b}l_2 = 1 \end{aligned} \quad (2-15)$$

So we can obtain the resonant frequency

$$\omega = \frac{1}{\sqrt{L_F C_F}} \quad (2-16)$$

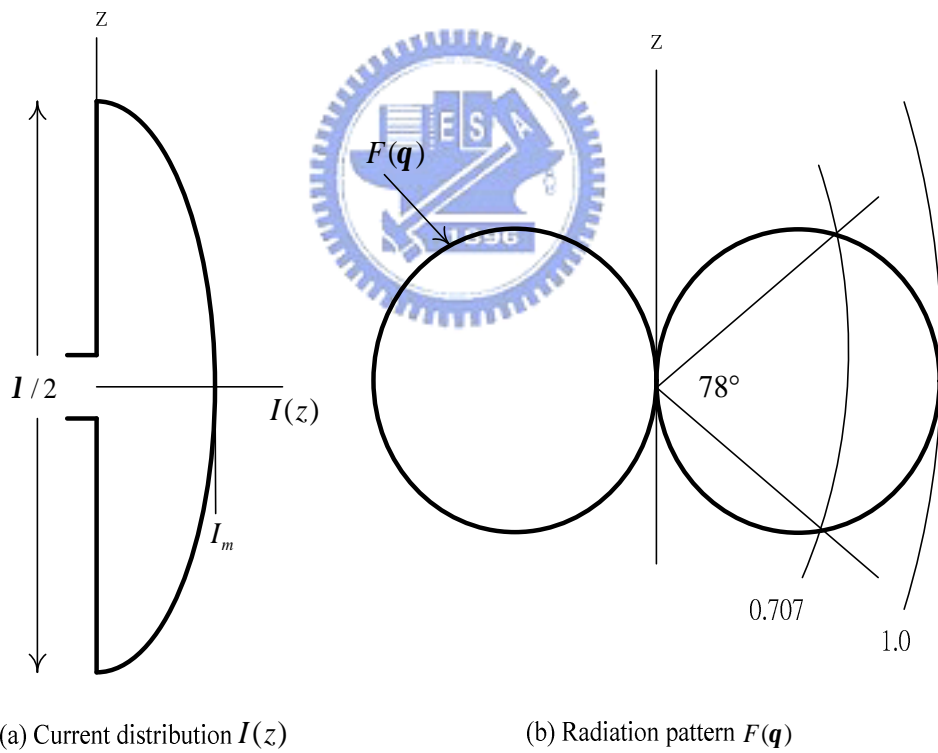


Figure 2-1: Current distribution and radiation pattern of the half-wave dipole

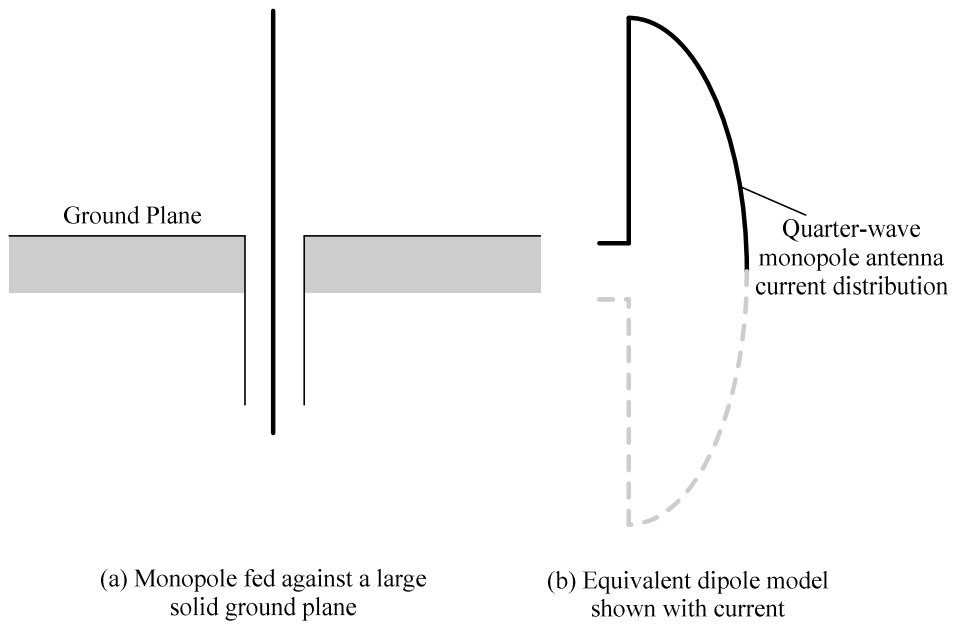


Figure 2-2: Monopole antenna fed against a ground plane with a coaxial cable

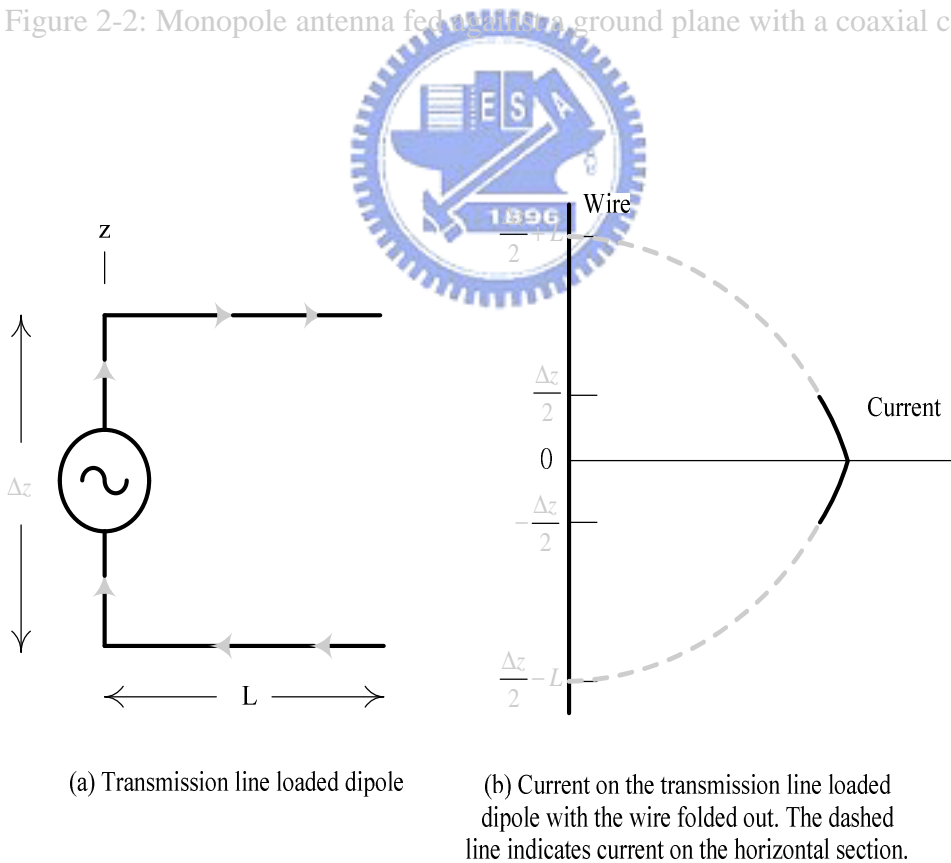


Figure 2-3: Transmission line loaded antenna

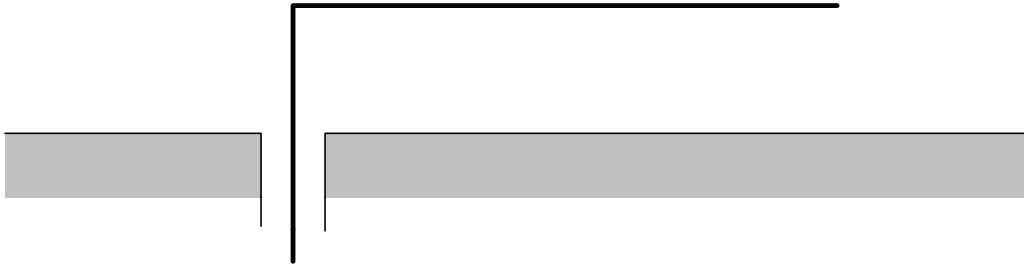
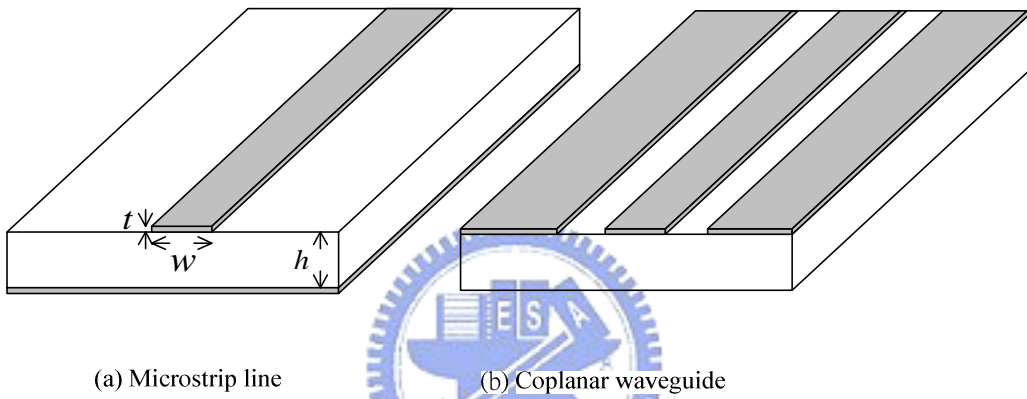


Figure 2-4: The inverted-L antenna



(a) Microstrip line

(b) Coplanar waveguide

Figure 2-5: Printed transmission lines

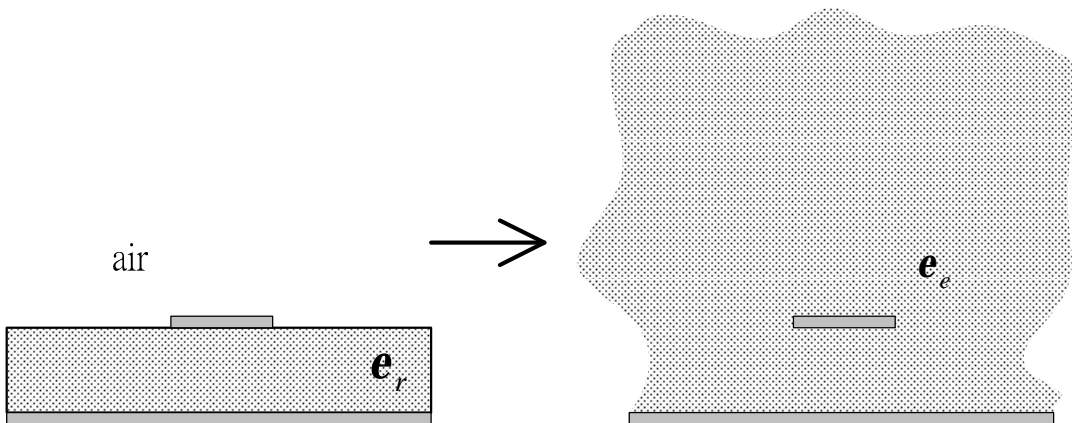
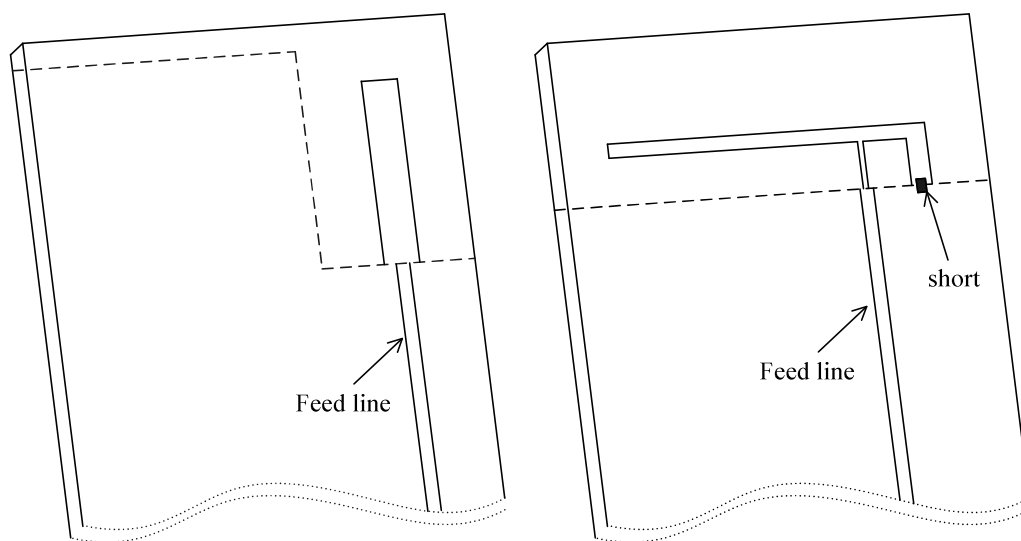


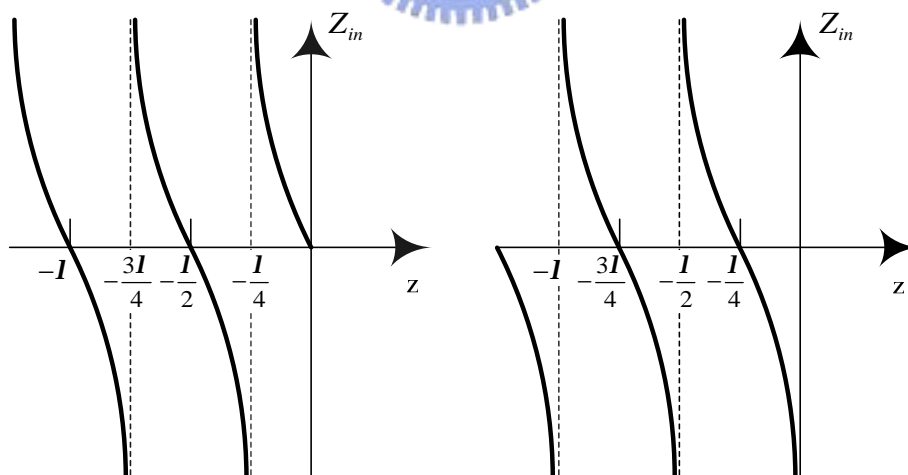
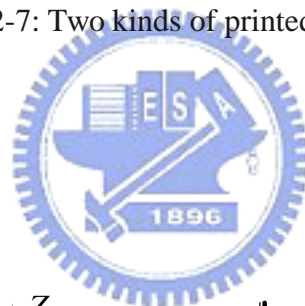
Figure 2-6: Quasi-TEM approximation



(a) Printed monopole antenna

(b) Printed inverted-F antenna

Figure 2-7: Two kinds of printed antennas



(a) impedance variation along a short-circuited transmission line

(b) impedance variation along an open-circuited transmission line

Figure 2-8: Impedance variation along a transmission line

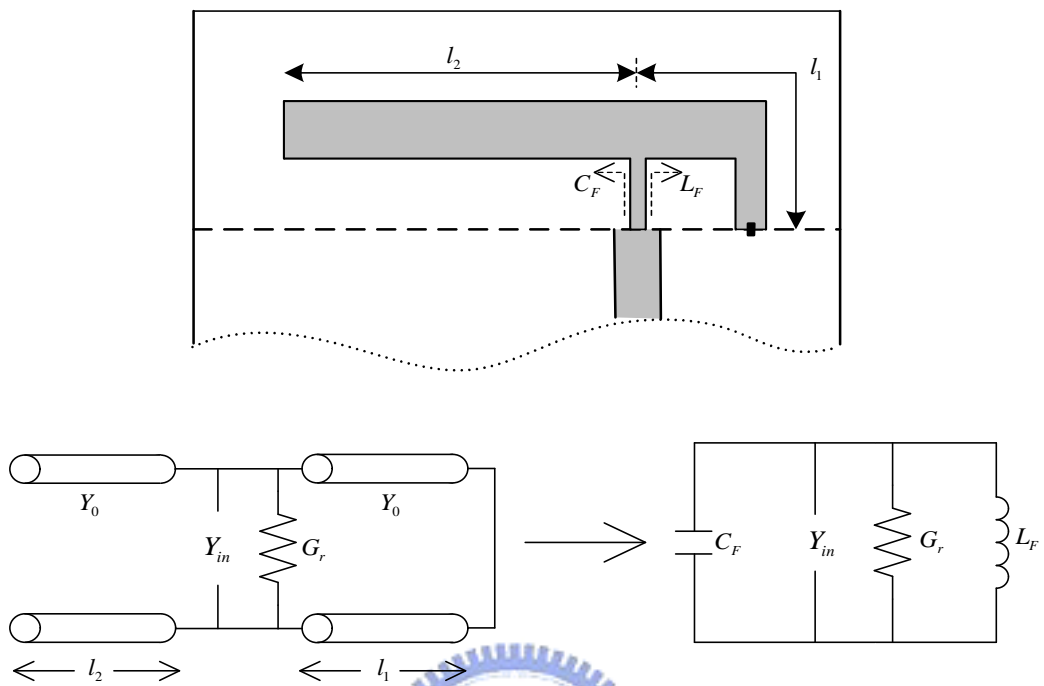
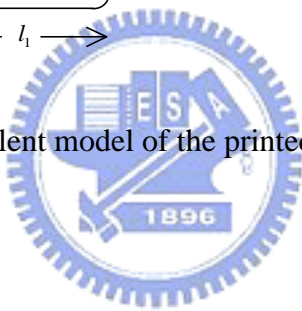


Figure 2-9: Equivalent model of the printed inverted-F antenna



Chapter 3: Design and Measurement of the Printed Inverted-E antenna

3.1 Design Theory

We will introduce a novel design about printed “inverted-E” antenna which is modified from the printed inverted-F antenna and has more compact structure. From the theory of the printed inverted-F antenna, we realize that the open end is like a capacitive load and if the length is longer, the equivalent capacitance is larger to induce a lower resonant frequency. Now we bend the open end toward the ground plane and protrude a metal line from the ground plane below the open end of the antenna as shown in Figure 3-1. It looks like a parallel plate capacitor which is connected to the open end of the antenna. Obviously, the structure will raise the equivalent capacitance to induce a lower resonant frequency without increasing the length of the antenna. The shape of this antenna is like a lying E letter, so we call it the printed “inverted-E” antenna. In [18], the similar idea was used in a modified PIFA with a capacitive load. But in this thesis, the printed inverted-E antenna has simpler manufacture process and more compact size.

The capacitive load C_L can reduce the antenna length as shown in Figure 3-2. The equivalent capacitance of the decreased length l_0 should be equal to capacitive load C_L . Hence we can obtain

$$j\omega C_L = jY_0 \tan \mathbf{b}(L - l_0) \quad (3-1)$$

and

$$C_L = \frac{Y_0}{\omega} \tan \mathbf{b}(L - l_0) \quad (3-2)$$

From this result, we can observe that the length L becomes shorter, the demand for the capacitive load C_L becomes larger. Consequently, larger capacitive load C_L results in a lower resonant frequency w of the antenna with the same length L .

3.2 Simulated and Measured Results

We accomplish the printed inverted-E antenna on the FR4 substrate, whose dielectric constant is 4.7, loss tangent is 0.02, and thickness is 0.8 mm. The ground size is 46.7 mm \times 88.8 mm. The feeding line is 50 μ m microstrip line. The EM numerical simulators used for this design are Zeland IE3D and Ansoft HFSS. Figure 3-3 shows the photography of the antenna with a size of 11mm \times 6.4mm. Figure 3-4 shows the simulated and measured return loss of the antenna. The 10dB bandwidth from 2.235 GHz to 2.57 GHz is 335 MHz. The measured result usually has 100 MHz downward offset to the simulated one. The result reveals that the antenna is suitable for 802.11b/g applications. Figure 3-5 shows the current density distribution of the antenna. The electrical length from the short point to the open end is $\lambda/4$. But because of the capacitive load, the physical length of the antenna is shorter than $\lambda/4$ of the EM wave propagating in the substrate. Figure 3-6 shows the measured radiation patterns of the antenna at 2.44 GHz. The maximum gain and average gain of X-Z, Y-Z and X-Y plane are listed below:

	X-Z plane	Y-Z plane	X-Y plane
Maximum Gain	0.19 dBi	2.08 dBi	-1.02 dBi
Average Gain	-0.97 dBi	0.04 dBi	-1.84 dBi

Table 3-1: The maximum and average gain of the printed inverted-E antenna in the X-Z, Y-Z and X-Y plane at 2.44 GHz.

Y-Z plane has not only nearly 0 dBi average gain and 2.09 dBi maximum gain larger than the other two cuts but also an omni-directional radiation pattern, so Y-Z plane has the best radiation performance between the three orthogonal planes.

The printed inverted-E antenna is used for the PCMCIA (personal computer memory card international association) card. The card has a case to protect the circuits on the PCB. The case may influence the radiation performance of the antenna, so we also measure the printed inverted-E antenna with a case. The photography of the printed inverted-E antenna with a case is shown in Figure 3-7. In practice, there is still an insulating material cover above the antenna in the photography. The simulated and measured return loss is shown in Figure 3-8. The 10dB bandwidth from 2.38 GHz to 2.62 GHz is 240 MHz. We can find that the case makes the resonant frequency have additional downward offset of 40 MHz. Figure 3-9 shows the measured radiation patterns of the antenna with a case at 2.44 GHz. The maximum gain and average gain of X-Z, Y-Z and X-Y plane are listed below:

	X-Z plane	Y-Z plane	X-Y plane
Maximum Gain	-1.29 dBi	1.40 dBi	1.43 dBi
Average Gain	-1.32 dBi	-0.51 dBi	-1.16 dBi

Table 3-2: The maximum and average gain of the printed inverted-E antenna with a case in the X-Z, Y-Z and X-Y plane at 5.77 GHz.

The case influences the radiation performance obviously. Note that the radiation patterns of Y-Z plane have several ripples because of the additional case. The gain and the radiation patterns of the X-Y plane with a case becomes better than that without a

case. The radiation patterns of the antenna with a case look like “pressed flat”. Figure 3-10 shows the measured gain as a function of the resonant frequency for the antenna without the case. The three curves imply a certain degree of each plane which has higher peak gain performance in the plane. Each curve of the three planes has little variation from 2.4 GHz to 2.4835 GHz.

3.3 Analysis

From Section 3.1, we know that the magnitude of parallel plate capacitance influences the resonant frequency of the antenna. So to change the parameter H_C can vary the resonant frequency of the antenna. Figure 3-11 shows the relationship between H_C and resonant frequency. When H_C becomes shorter, the equivalent capacitive load becomes smaller so that the resonant frequency becomes higher. Although the increase of H_C results in a lower resonant frequency or smaller antenna size, it is impossible to reduce the size without constraints. There are two reasons. One is that a larger capacitance demands a smaller inductance to resonate at the same frequency from (2-16). Smaller inductance means the shorter short-circuited transmission line or the wider width of the transmission line. It has some limitations to shorten or thin the transmission line so that the inductance has a minimum value in practical fabrication. The other reason is Q-value of the antenna. From [15], the Q-value is defined as $2pf$ times the peak energy stored/average power radiated. Practically speaking, high Q means that the input impedance is very sensitive to the small changes in frequency. The Q definition of antenna is similar to the circuit theory. From [17], the Q of the parallel RLC resonant circuit can be expressed as

$$Q = \omega_0 RC \quad (3-3)$$

where ω_0 is the center resonant frequency of the resonator. So larger capacitance induces higher Q and the bandwidth becomes narrower. The capacitive load of the

printed inverted-E antenna will cause the Q-value to rise rapidly and reduce the bandwidth of the antenna. Hence, the increasing Q with diminishing size implies a fundamental limitation on the usable bandwidth of the antenna. High Q and small bandwidth are specific limitations of small antennas.

We establish the equivalent circuit model for printed inverted-E antenna. First, we remove the capacitive load of the antenna. This structure is simulated by Zeland IE3D. The dash line of Figure 3-13 is the simulated return loss of the antenna without capacitive load. The antenna without capacitive load is actual a short printed inverted-F antenna whose resonant frequency is about 4.2 GHz. From Section 2.5, we know the equivalent circuit model of the printed inverted-F antenna is a RLC resonator. So, we use Microwave Office to simulate a RLC circuit as shown in Figure 3-12, and let the simulated return loss of the circuit fit the previously simulated return loss curve of the short printed inverted-F antenna as shown in Figure 3-13. The return loss of the antenna seems to have other resonant frequencies but the equivalent circuit does not. It is because that the non-dominant modes induce other resonant frequencies. To fit the curve better, we can add other RLC resonators to represent the non-dominant modes but it will increase the complexity of the equivalent circuit.

To complete the equivalent circuit mode of the printed inverted-E antenna, we connect an additional capacitor to the RLC resonator and wish that can fit the previously simulated return loss curve of the printed-E antenna. But there is still impedance mismatching between two curves. In addition to the capacitor, we further shunt a resistance to the RLC resonator as shown in Figure 3-14. The fitted curve is shown in Figure 3-15. Obviously, the additional resistance behaves as the leakage current in the parallel plate capacitor. The wider bandwidth of the antenna is also cause by the non-dominant mode as well as the above discussion.

If we remove the capacitive load and only adjust the length of the open arm. We

should obtain a printed inverted-F antenna resonated in the same frequency as the printed inverted-E antenna. Figure 3-16 shows the return loss of the two antennas. The printed inverted-F antenna is impedance mismatching even if it has the same resonant frequency. Furthermore, the open arm of the printed inverted-F antenna is almost twice as long as the one of the printed inverted-E antenna. So, the printed inverted-E antenna is a compact antenna for WLAM applications.

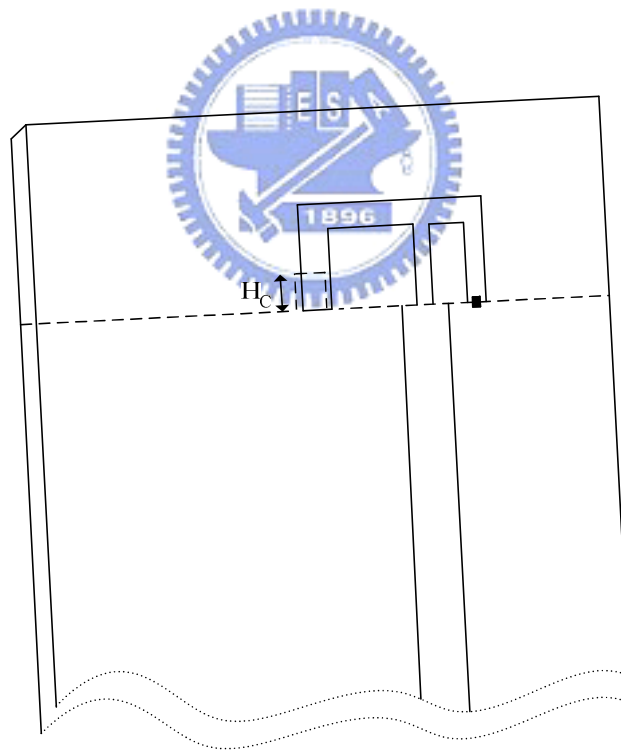


Figure 3-1: Geometry of the printed inverted-E antenna

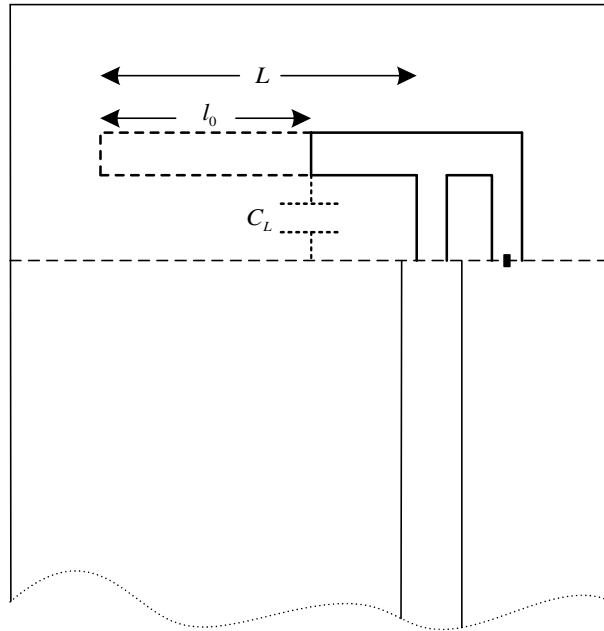


Figure 3-2: Equivalent capacitance of the decreased length equals the capacitive load

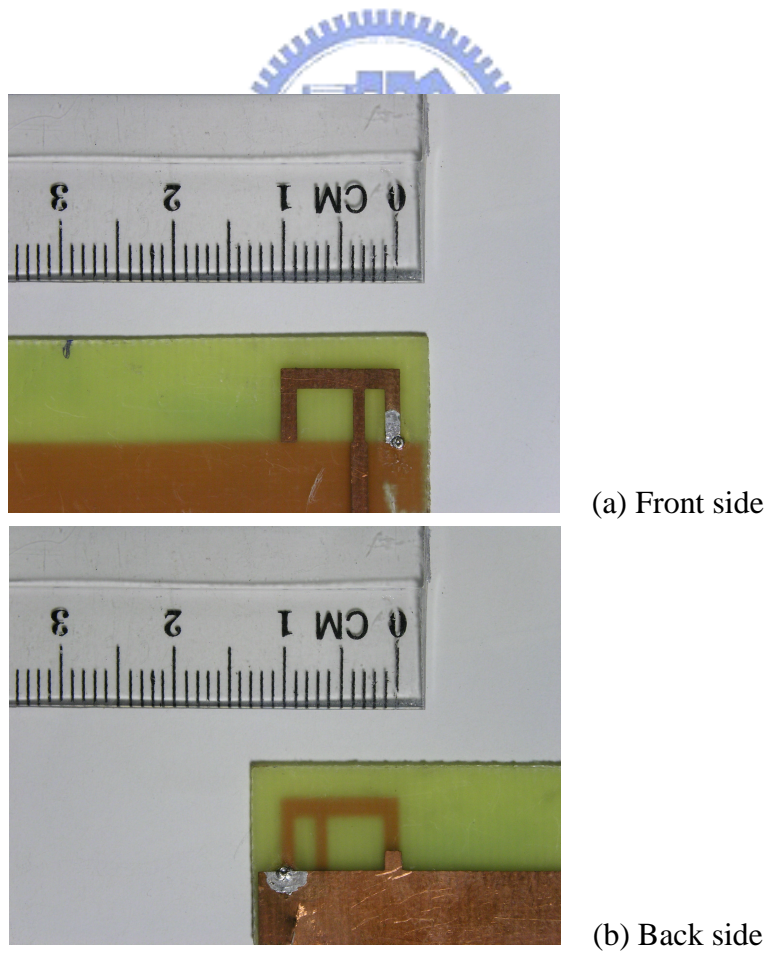


Figure 3-3: Photography of the printed inverted-E antenna

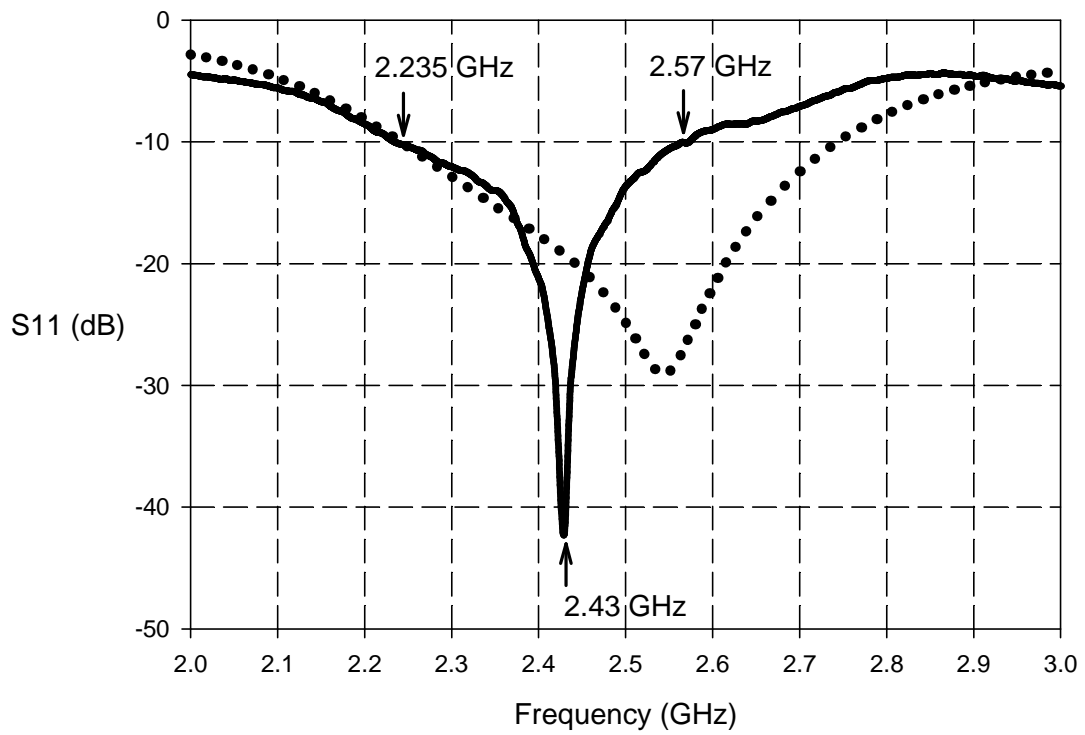
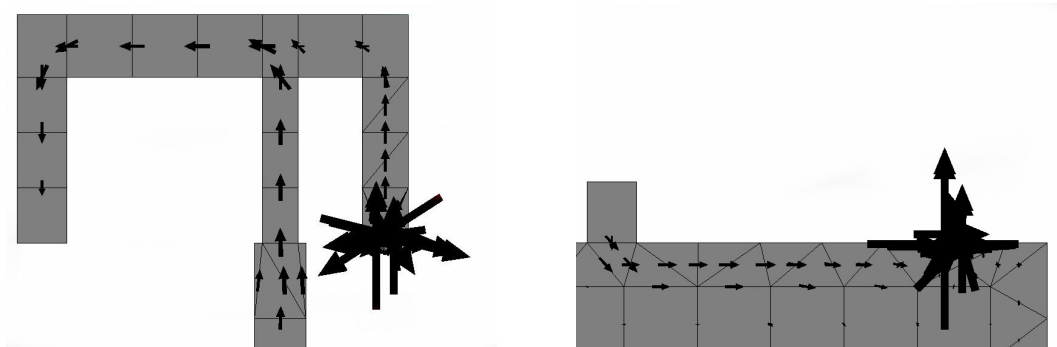


Figure 3-4: Simulated and measured return loss of the printed inverted-E antenna



(a) Front side

(b) Back side

Figure 3-5: Current density distribution of the inverted-E antenna

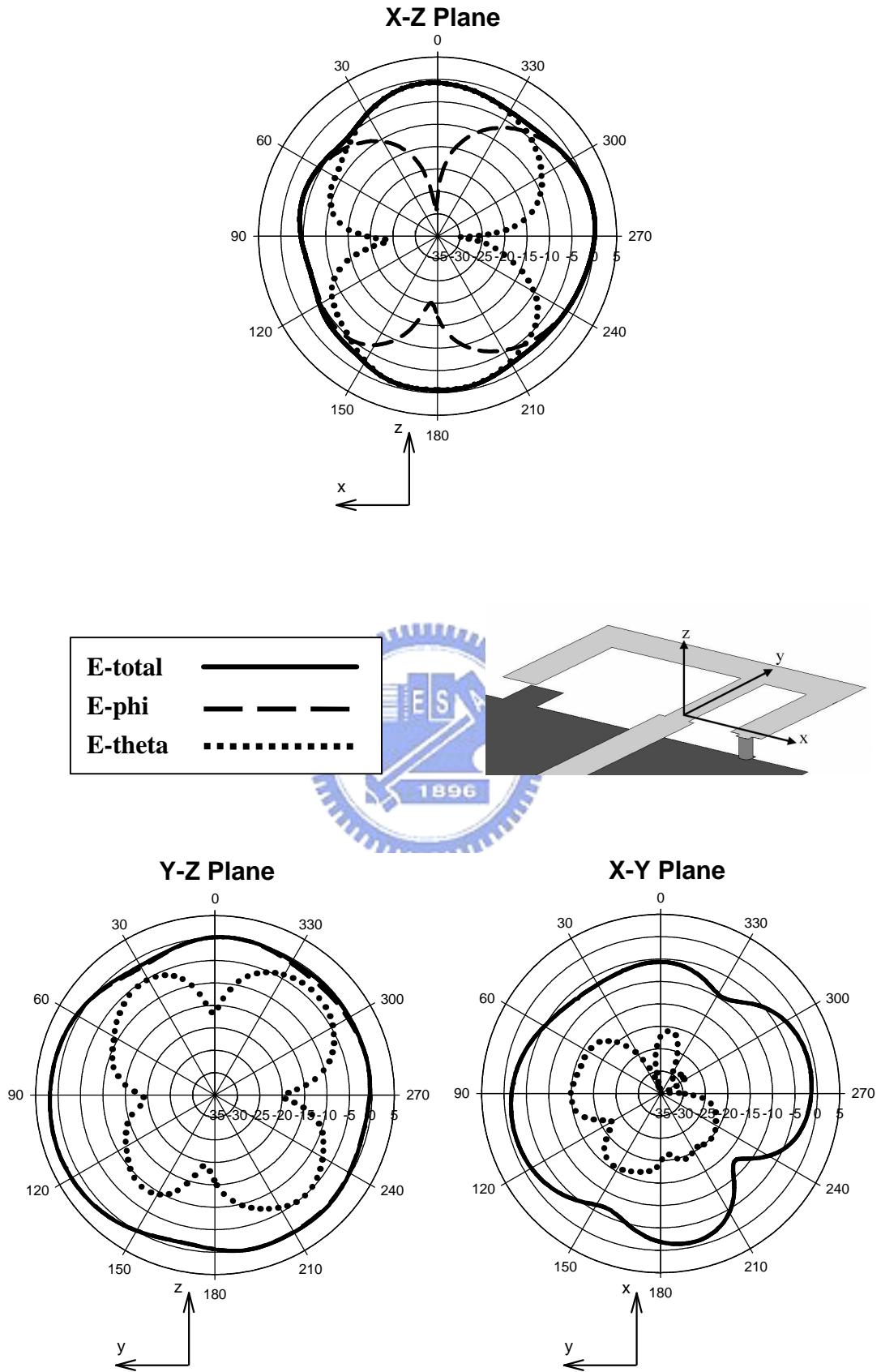


Figure 3-6: Measured radiation patterns of the printed inverted-E antenna at 2.44 GHz

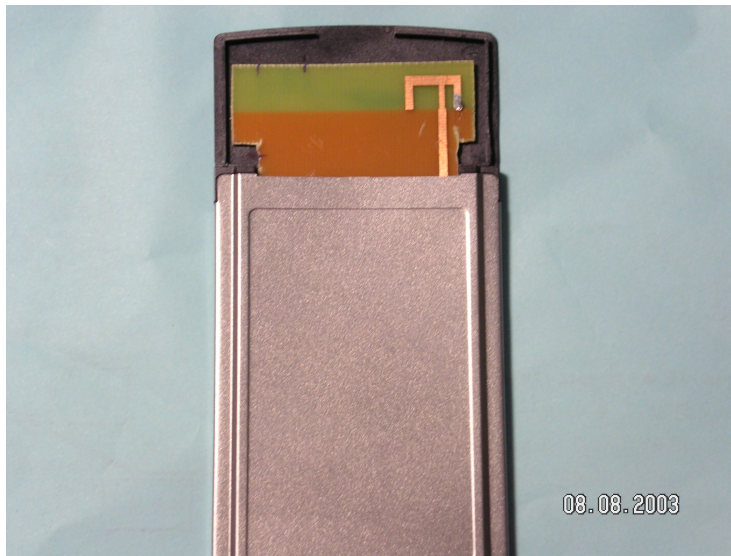


Figure 3-7: Photography of the printed inverted-E antenna with a case

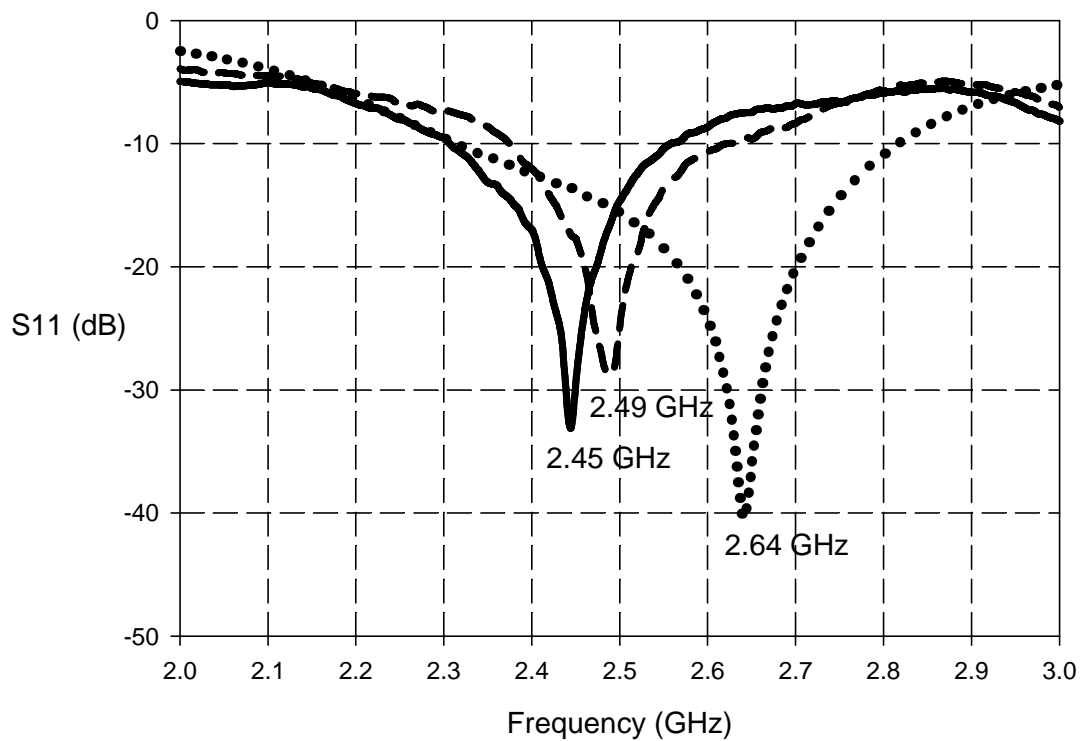


Figure 3-8: Simulated and measured return loss of the printed inverted-E antenna with a case

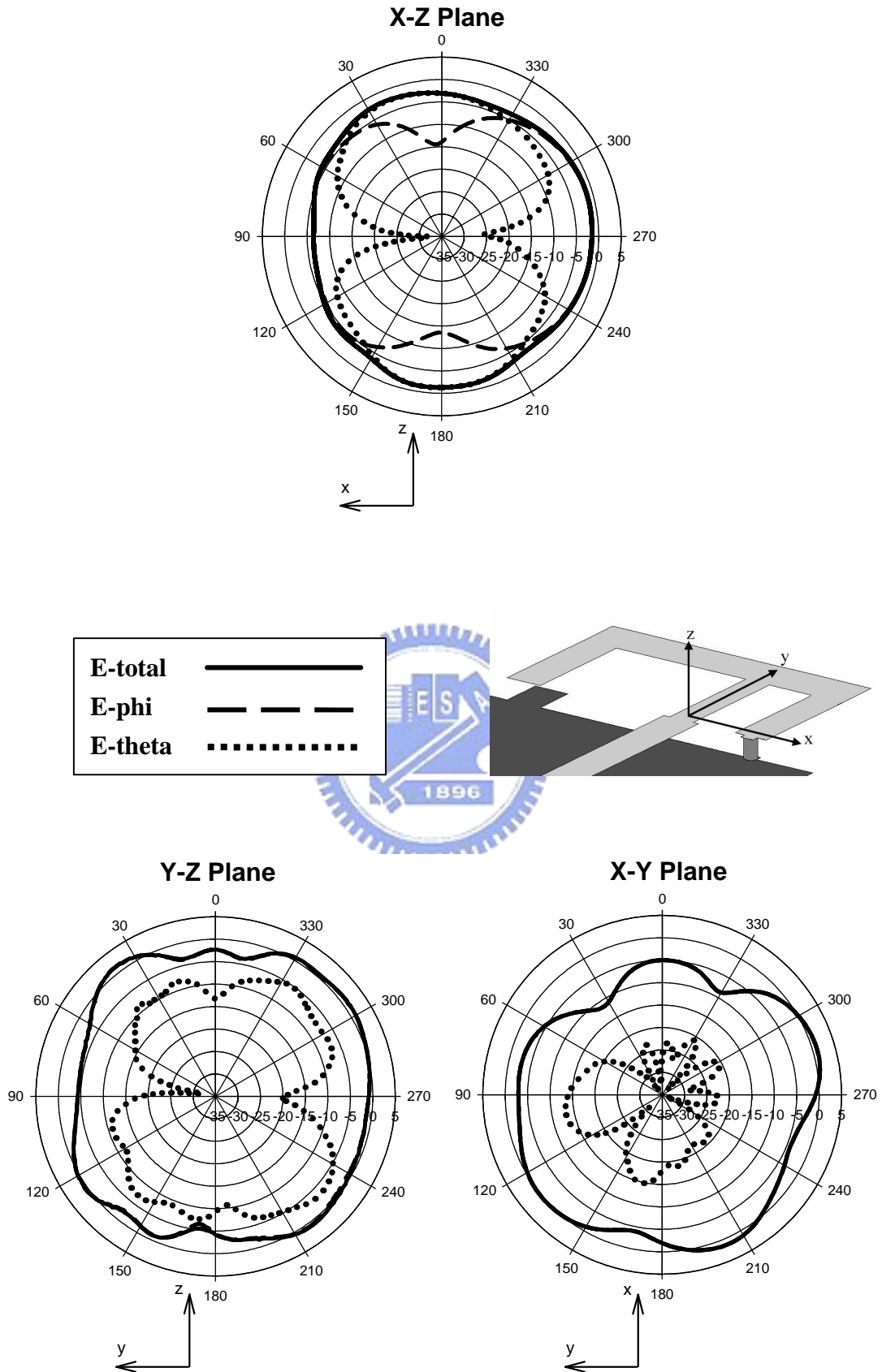


Figure 3-9: Measured radiation patterns of the printed inverted-E antenna with a case at 2.44 GHz

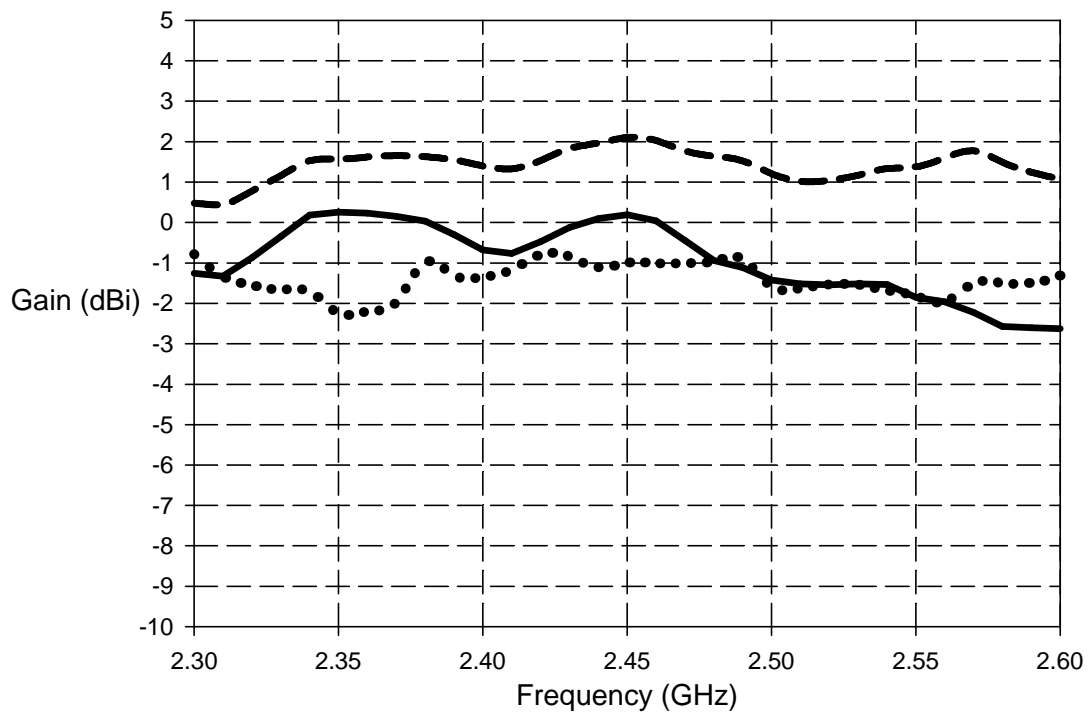


Figure 3-10: Measured gain of the printed inverted-E antenna versus frequency

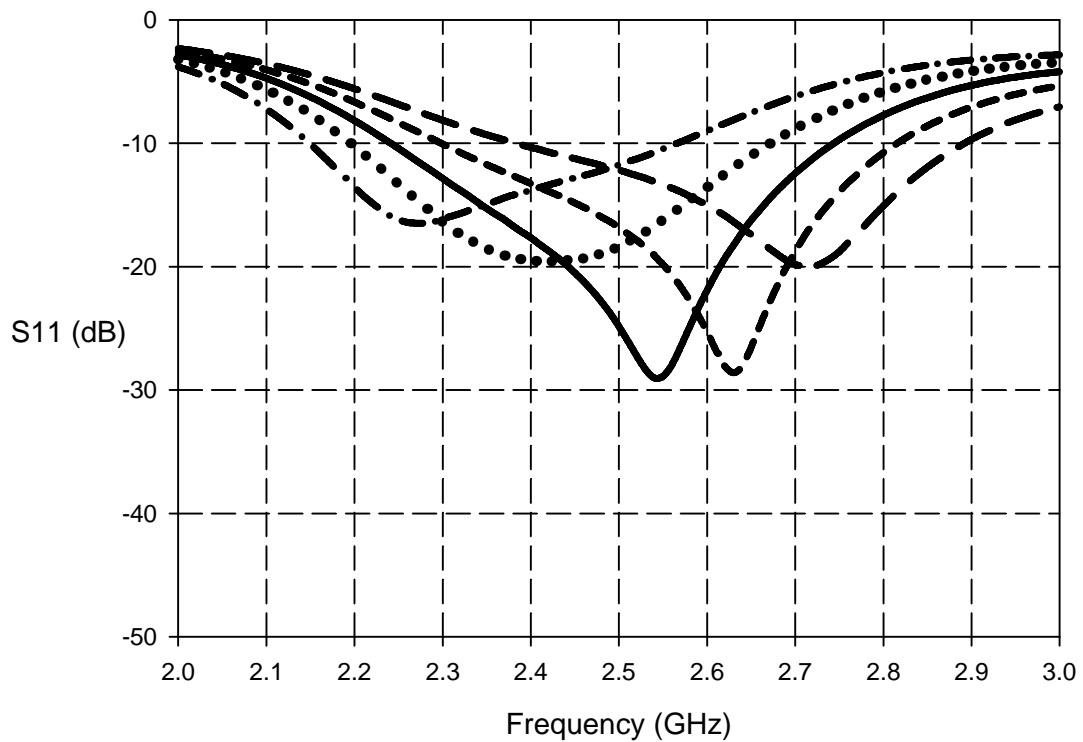


Figure 3-11: Simulated return loss versus frequency for different H_C

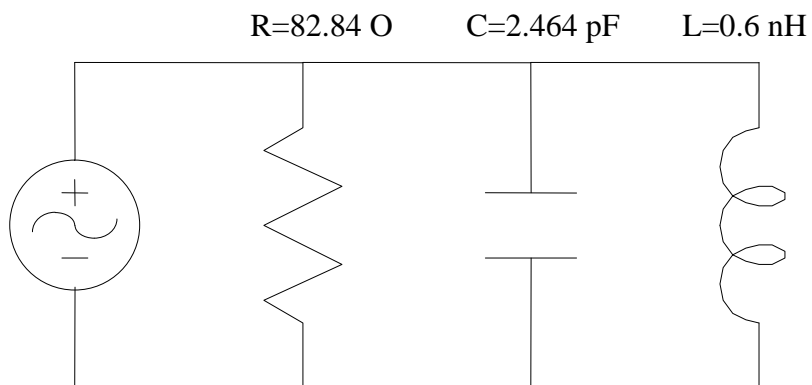


Figure 3-12: Equivalent circuit model of the printed inverted-E antenna without the capacitive load

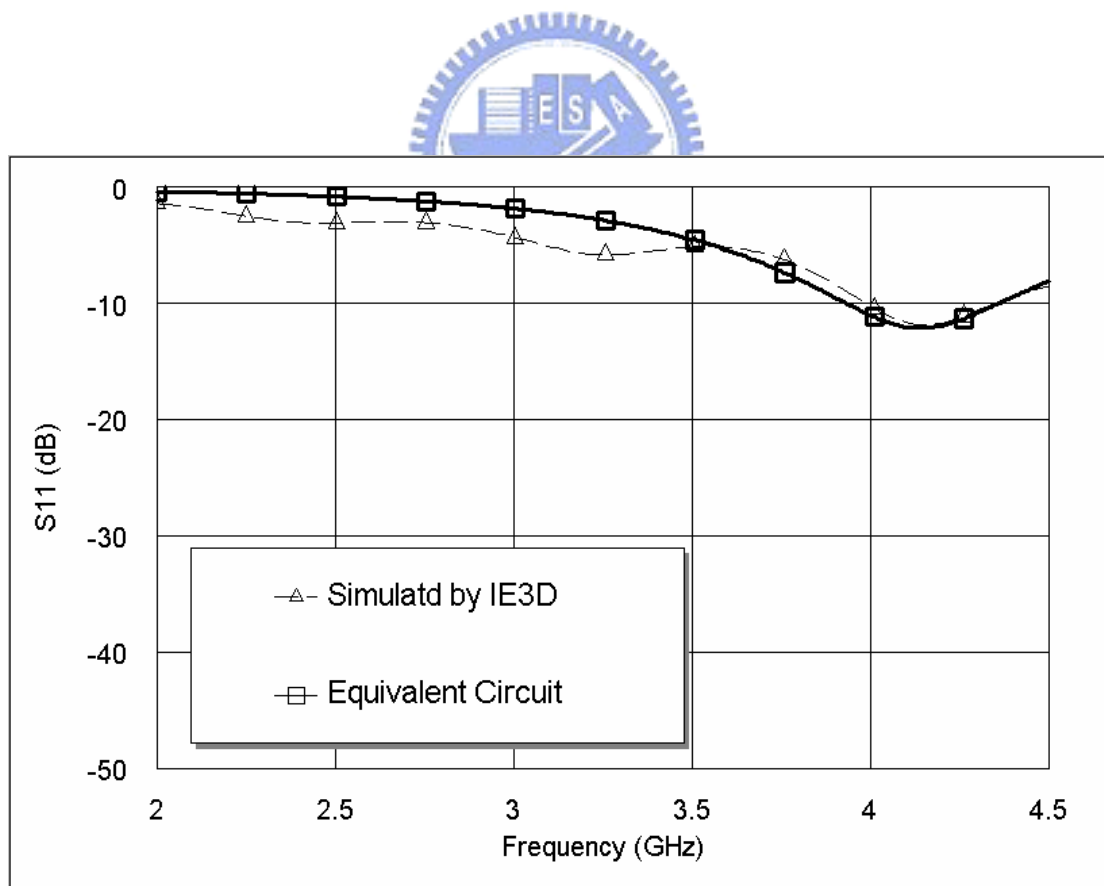


Figure 3-13: Return loss of the equivalent circuit in Figure 3-12

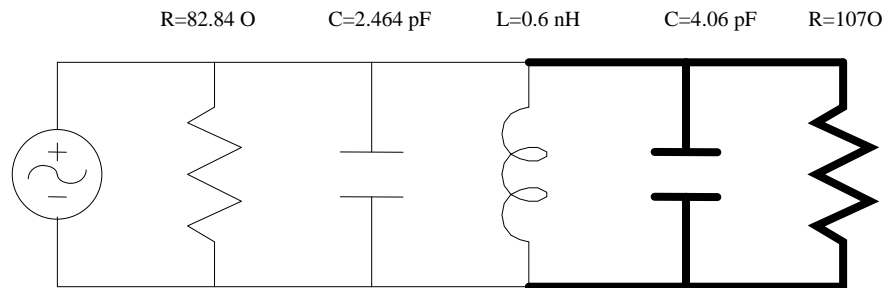


Figure 3-14: Equivalent circuit of the printed inverted-E antenna

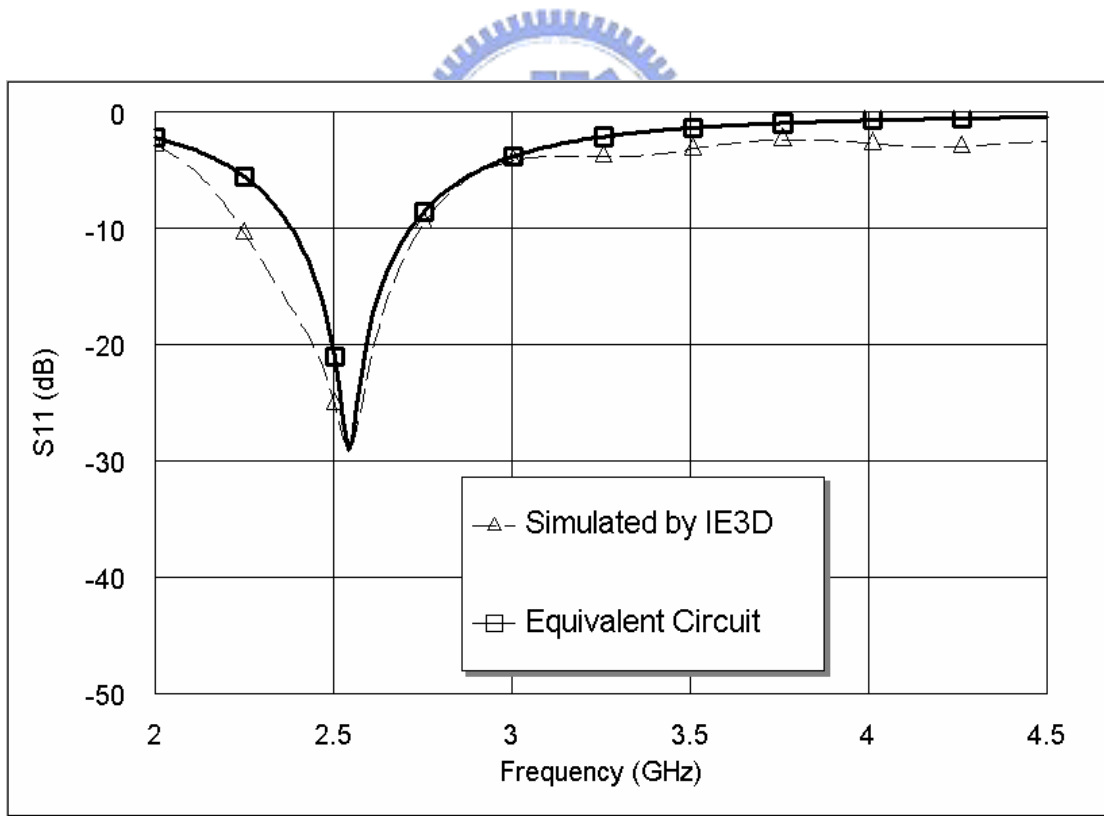


Figure 3-15: Return loss of the equivalent circuit in Figure 3-14

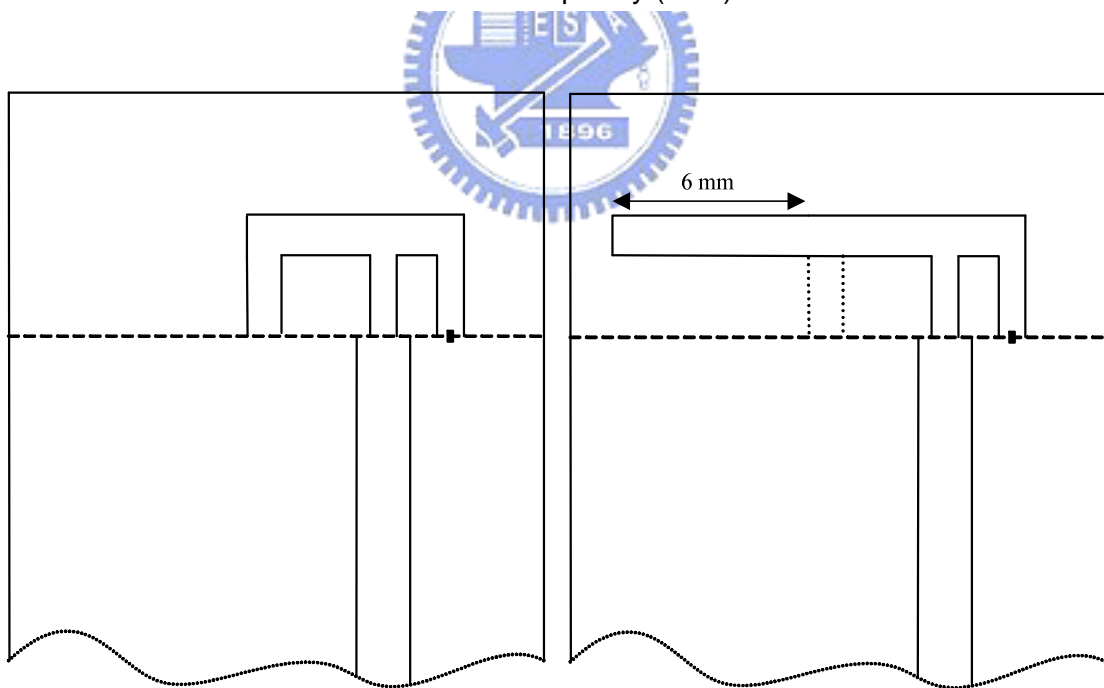
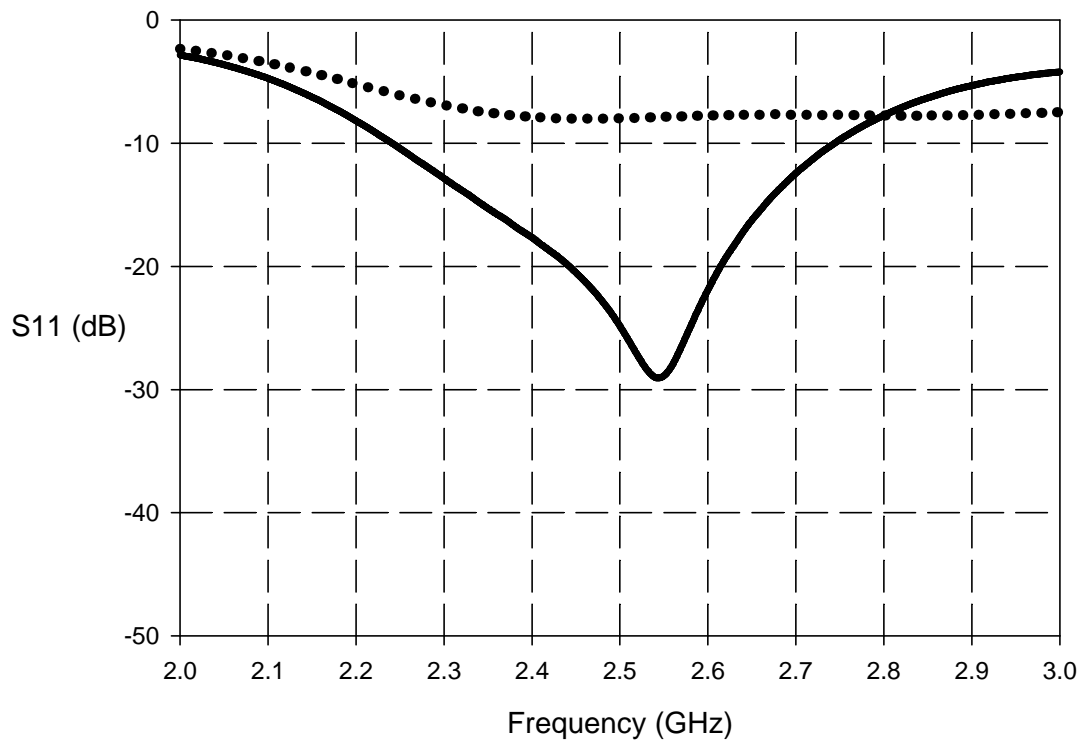


Figure 3-16: Return loss of the printed inverted-E and inverted-F antenna at the same resonant frequency

Chapter 4: Design and Measurement of a Dual-Band Monopole Antenna with a Microstrip Choke

4.1 Design Theory

Now we review the transmission line theory discussed in the Section 2.5 first. The input impedance Z_{in} of a short-circuited transmission line with length l is

$$Z_{in} = jZ_0 \tan \beta l \quad (4-1)$$

When the length l equals to $\lambda/4$, the input impedance is infinite. Therefore, the input impedance of this transmission line is open-circuited. According to this idea, we connect one terminal of a short-circuited transmission line to the end of a typical monopole antenna, and the other terminal of the transmission line is connected to a tuning metal line. The schematic diagram is shown in Figure 4-1. In the present design, the transmission-line length l is set as a quarter-wavelength at a higher frequency similar to the resonant frequency of the typical monopole antenna. From (4-1), the input impedance of the short-circuited transmission line is infinite for higher frequency signal. Thus, at the resonant frequency the current flowing on the typical monopole antenna and the transmission line is difficult to enter the tuning metal line. This means that the length of the tuning line has little influence on the radiation performance of the typical monopole antenna. Therefore, the short-circuited transmission line performs as a “choke” at higher frequency. For the lower frequency signal, the short-circuited transmission line is not open at the input end because the length is no longer quarter wavelength. The antenna now behaves like a bent monopole antenna at lower frequency with its electrical length from the input point of the 5GHz monopole antenna, through the short-circuited transmission line, to the end of the tuning line. The length of the tuning line is tuned to make the total length of the

bent monopole antenna near a quarter-wavelength so as to be resonant. Hence, the antenna has a simple structure but it can be used in dual-band applications.

4.2 Simulated and Measured Results

Figure 4-2 shows the structure of the dual-band antenna accomplished on a FR4 substrate, whose dielectric constant is 4.7, loss tangent is 0.02, and thickness is 0.8 mm. The size of the ground is 46.7 mm × 88.8 mm. The feeding line is a 50 microstrip line. The EM numerical simulators are Zeland IE3D and Ansoft HFSS. The structure of the antenna has three separate parts: a monopole antenna, a short-circuited transmission line, and a tuning end. The first part performs as a general printed monopole antenna at 5 GHz, which has a metal trace length equal to a quarter-wavelength at 5 GHz. The second part is a short-circuited transmission line with the input port connected to the 5 GHz printed monopole antenna and the tuning end in series.

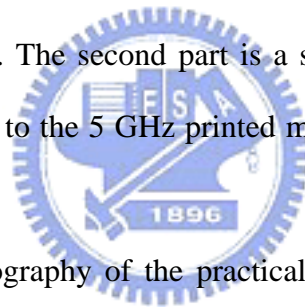


Figure 4-3 is the photography of the practical dual-band antenna. Figure 4-4 shows both the simulated and measured return loss of the dual-band antenna. It is observed that the dual-band antenna exhibits two resonant bands at 2.4GHz and 5 GHz. The 10 dB bandwidth at 2.4 GHz is 350 MHz, which is from 2.35 GHz to 2.7 GHz. The 10 dB bandwidth of 5 GHz is 1.05 GHz, which is from 4.68 GHz to 5.73 GHz. The antenna is suitable for 802.11 a/b/g applications. Figure 4-5 shows the simulated current density distribution in the two operating bands. Obviously, the 5 GHz monopole antenna sees large impedance in the terminal position, thus rare current can enter the tuning metal line. In the other hand, the current density distribution from the feed point to the end of the tuning line at 2.4GHz behaves like a quarter-wavelength monopole antenna. To be compared with the dual band antenna, we also design a 2.4GHz typical monopole antenna as shown in Figure 4-6. Figure

4-7 shows the measured radiation patterns of the dual-band antenna at 2.44 GHz. The maximum gain and average gain of X-Z, Y-Z and X-Y plane are listed below:

	X-Z plane	Y-Z plane	X-Y plane
Maximum Gain	-1.45 dBi	2.43 dBi	1.43 dBi
Average Gain	-1.96 dBi	-1.19 dBi	-1.17 dBi

Table 4-1: The maximum and average gain of the dual-band antenna in the X-Z, Y-Z and X-Y plane at 2.44 GHz.

The measured patterns of an ordinary 2.4GHz printed monopole antenna on the same ground size is also shown in Figure 4-8 for comparison. The maximum gain and average gain of X-Z, Y-Z and X-Y plane are listed below:

	X-Z plane	Y-Z plane	X-Y plane
Maximum Gain	-4.19 dBi	2.52 dBi	2.10 dBi
Average Gain	-2.78 dBi	-0.96 dBi	-0.97 dBi

Table 4-2: The maximum and average gain of the typical monopole antenna in the X-Z, Y-Z and X-Y plane at 2.44 GHz.

The maximum gain of the dual-band antenna at 2.44 GHz is a bit smaller than of the ordinary one and we can see that the radiation patterns are almost omni-directional and are very similar between the two antennas. Thus, the short-circuited transmission line performs little influence at lower band of the new antenna. The ground width is only about twice as the antenna length, so the ground plane is not a perfect image plane. The edge current of the ground will also radiate, so that they influence the

radiation performance of the antenna. Hence, the notches in the E-plane (Y-Z plane and X-Y plane) of the above two antennas are caused by the ground edge current. Figure 4-9 shows the measured radiation patterns of the dual-band antenna at 5.25 GHz. The maximum gain and average gain of X-Z, Y-Z and X-Y plane are listed below:

	X-Z plane	Y-Z plane	X-Y plane
Maximum Gain	2.32 dBi	1.68 dBi	4.58 dBi
Average Gain	0.03 dBi	-0.70 dBi	-0.39 dBi

Table 4-3: The maximum and average gain of the dual-band antenna in the X-Z, Y-Z and X-Y plane at 5.25 GHz.

The radiation patterns are also omni-directional at this band. Note in the Y-Z plane, the E-phi component is larger than the E-theta component, in average. We can thus infer that the short-circuit transmission line has large influence on the radiation patterns. Figure 4-10 shows the measured radiation patterns of the dual-band antenna at 5.77 GHz. The maximum gain and average gain of X-Z, Y-Z and X-Y plane are listed below:

	X-Z plane	Y-Z plane	X-Y plane
Maximum Gain	3.07 dBi	3.38 dBi	3.78 dBi
Average Gain	-0.54 dBi	-0.07 dBi	-1.38 dBi

Table 4-4: The maximum and average gain of the dual-band antenna in the X-Z, Y-Z and X-Y plane at 5.77 GHz.

The X-Y plane pattern at 5.77 GHz is poorer than 5.25 GHz. There are obvious nulls in the right side of the antenna.

Even if the antenna can work in dual band, it does not reduce the antenna size obviously. The bent tuning metal line can reduce the antenna size like the inverted-L antenna. We put the modified antenna in a $15\text{mm}\times 15\text{mm}$ region which is surrounded by ground plane. The photography of the modified antenna is as shown in Figure 4-11. The left region without ground plane will also put another antenna in. But it is not in the discussed range in this thesis. The simulated and measured return loss is as shown in Figure 4-12. The 10 dB bandwidth at 2.4 GHz is 520 MHz, which is from 2.23 GHz to 2.75 GHz. The 10 dB bandwidth of 5 GHz is 1.12 GHz, which is from 4.78 GHz to 5.9 GHz. The antenna put in the horizontal direction will have better radiation performance. Since the longer wavelength of 2.4 GHz EM wave, the current will be induced on the both size of the protruding ground plane by the coupling of the antenna and is in phase. Hence, the protruding ground plane and the modified antenna are like a two elements Yagi-Uda antenna and the protruding ground plane works like a parasite. So the pattern shape looks like a wide beam direct to the protruding plane and weak radiation pattern against the direction of ground plane, particularly in X-Y plane. It is not a good radiation pattern for the omni-directional antenna. The horizontal form will improve the radiation patterns very much in lower frequency. As in the 5 GHz band, if the antenna is put in vertical direction, the antenna only couples with near side of the ground plane and they work like a transmission line. So the radiation patterns are weak in the ground plane direction. It is also a disadvantage to put the antenna in vertical direction. Figure 4-13 shows the measured radiation patterns of the modified dual-band antenna at 2.44 GHz. The maximum gain and average gain of X-Z, Y-Z and X-Y plane are listed below:

	X-Z plane	Y-Z plane	X-Y plane
Maximum Gain	-2.10 dBi	2.65 dBi	3.59 dBi
Average Gain	-2.30 dBi	-1.17 dBi	-1.27 dBi

Table 4-5: The maximum and average gain of the modified dual-band antenna in the X-Z, Y-Z and X-Y plane at 2.44 GHz.

There are more ripples than the original dual-band antenna as each ground edge current. But the radiation patterns are improved more than the antenna put in the vertical direction. Figure 4-15 shows the measured radiation patterns of the dual-band antenna at 5.25 GHz. The maximum gain and average gain of X-Z, Y-Z and X-Y plane are listed below:

	X-Z plane	Y-Z plane	X-Y plane
Maximum Gain	2.17 dBi	6.17 dBi	6.60 dBi
Average Gain	-0.73 dBi	0.44 dBi	-0.52 dBi

Table 4-6: The maximum and average gain of the modified dual-band antenna in the X-Z, Y-Z and X-Y plane at 5.25 GHz.

The shape of the radiation patterns are not like the antenna put in vertical direction as above discussion. The radiation patterns are like toward the ground plane. Thus it can be seen that the choke has remarkable radiation performance just like the original dual-band antenna discussed above. So the choke now is like a driver of the “quasi-Yagi-Uda” antenna. Figure 4-16 shows the measured radiation patterns of the dual-band antenna at 5.77 GHz. The maximum gain and average gain of X-Z, Y-Z and

X-Y plane are listed below:

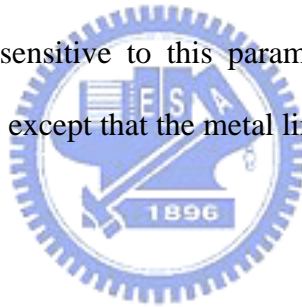
	X-Z plane	Y-Z plane	X-Y plane
Maximum Gain	2.79 dBi	5.74 dBi	6.39 dBi
Average Gain	-0.89 dBi	0.50 dBi	-0.39 dBi

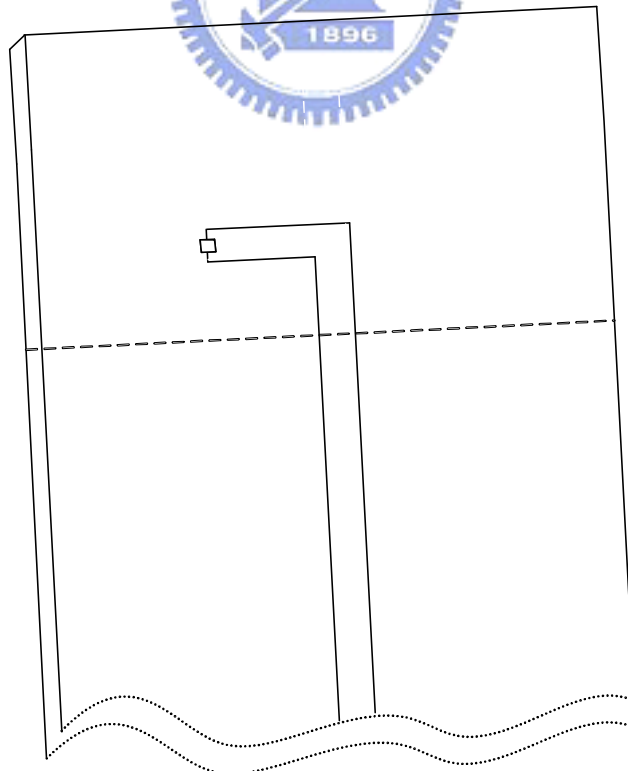
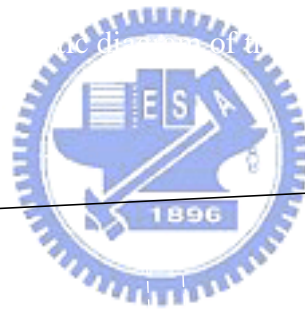
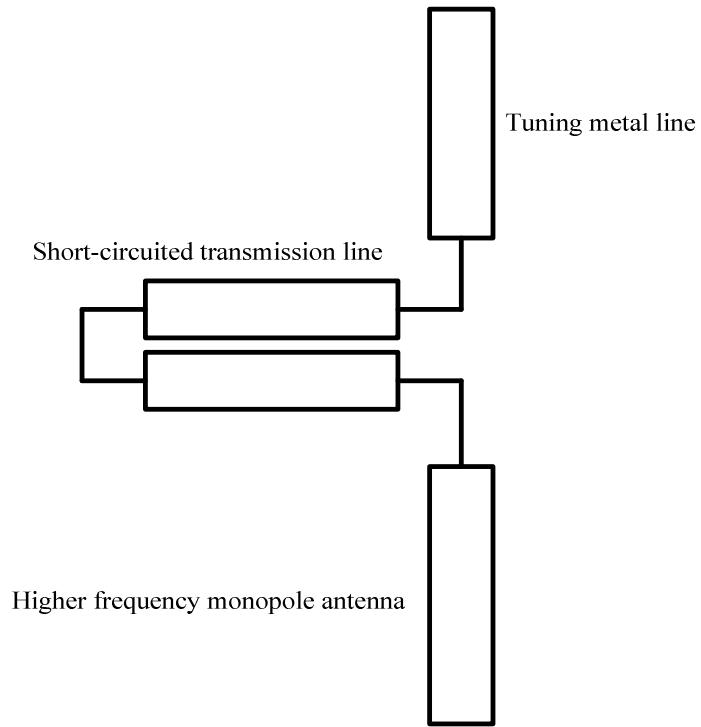
Table 4-7: The maximum and average gain of the modified dual-band antenna in the X-Z, Y-Z and X-Y plane at 5.77 GHz.

4.3 Analysis

Now we show a design flow and illustrate how to design this dual-band monopole antenna step by step. We fabricate the three parts of the dual-band antenna respectively and then connect them to each other as shown in Figure 4-17. First, we simulate a typical printed monopole antenna and let it have higher resonant frequency such as 5 GHz. At this step, using the inverted-L antenna is admitted. The dash line as shown in the Figure 4-18 is the return loss of the 5 GHz typical monopole antenna. Second, we will design the choke. For the purpose of convenience, we choose the ground width to be the same as the signal width. It is more like the parallel plate transmission line than microstrip line. Since it is fabricated on the PCB, we also call it the microstrip choke. Certainly, the signal width of a choke which is different to the ground width is admitted. The configuration of the choke can be straight line, bent line, spiral line or etc, as shown in Figure 4-19. Here we choose the straight line at this step. We simulate the choke and let the Z-parameters be infinite at 5 GHz. Note the Figure 4-17, since the intersection contact between three parts of the antenna is not a point, the length of the choke in the simulation must include the intersection contact. It is an experience rule. The dot line as shown in the Figure 4-18 is the

Z-parameters of the choke. Finally, we connect the choke to the end of the typical monopole antenna and the other terminal of the choke is connected to a proper length of a metal line. The solid line shown as in Figure 4-18 is the return loss of whole antenna which has dual-band performance. The high frequency may have some offset. If we design at the lower frequency and with a simpler structure, the result will be less offset. Similar to the above, the choke can have several shapes as shown in Figure 4-19. If we all let the input impedance of the three shapes infinite at the same frequency and the part of the typical monopole antenna and the tuning line is the same for the three chokes, the simulated return loss of the three chokes are shown in Figure 4-20. The result is similar to each antenna with different choke. If we only vary the tuning metal line length of the antenna, the result will be shown in Figure 4-21. The lower resonant frequency is sensitive to this parameter and the bandwidth of the higher band has little variation except that the metal line is too long.





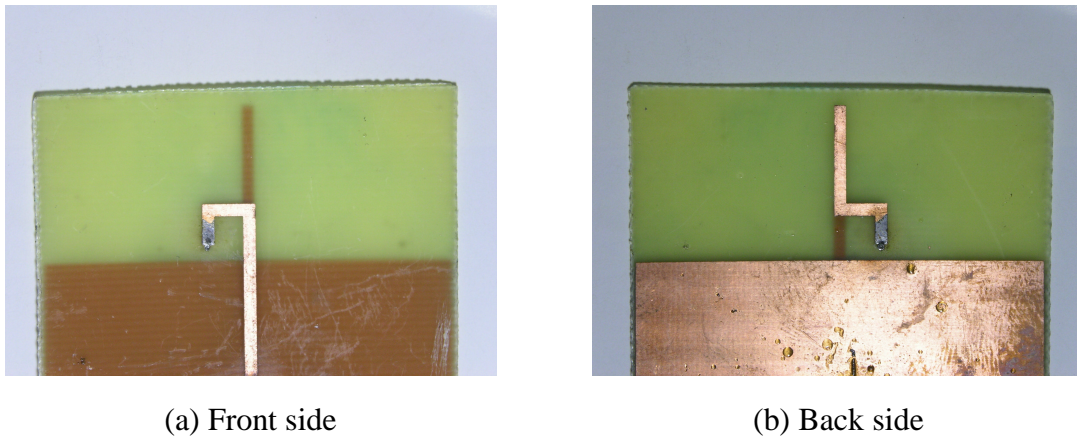


Figure 4-3: Photography of the dual-band antenna

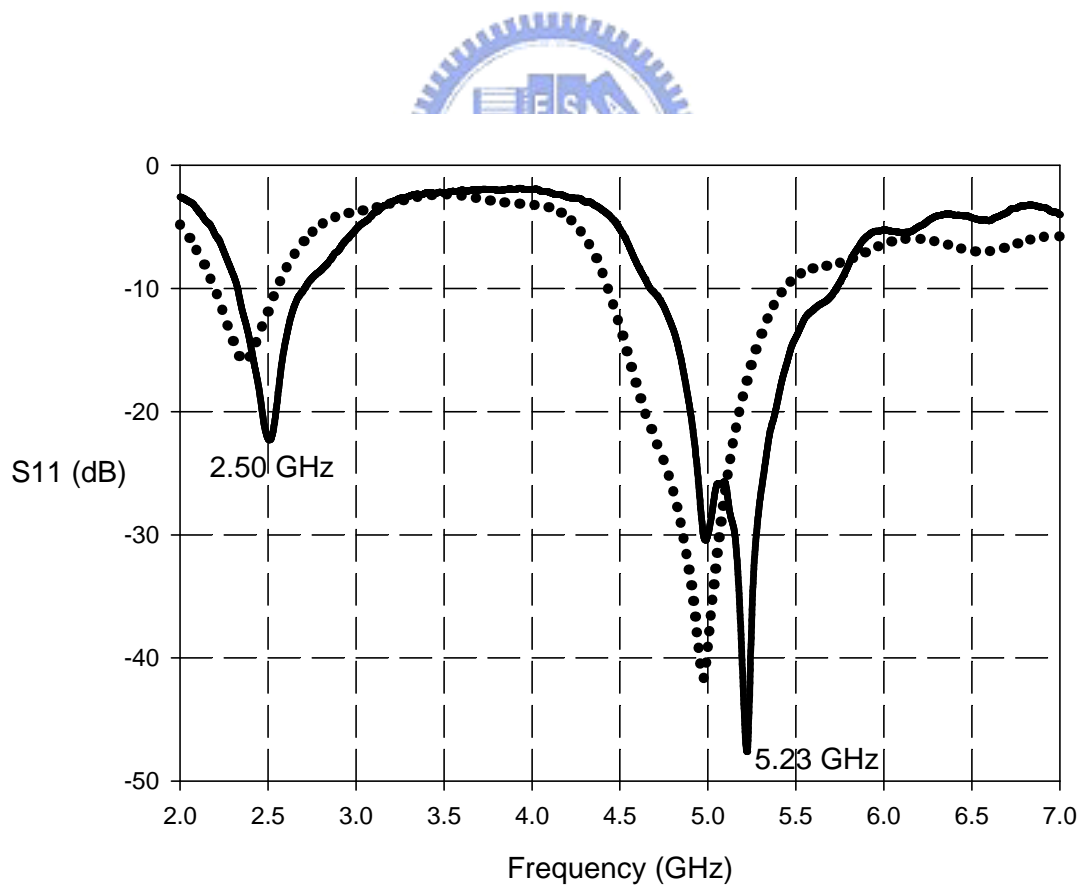


Figure 4-4: Measured and simulated return loss of the dual-band antenna

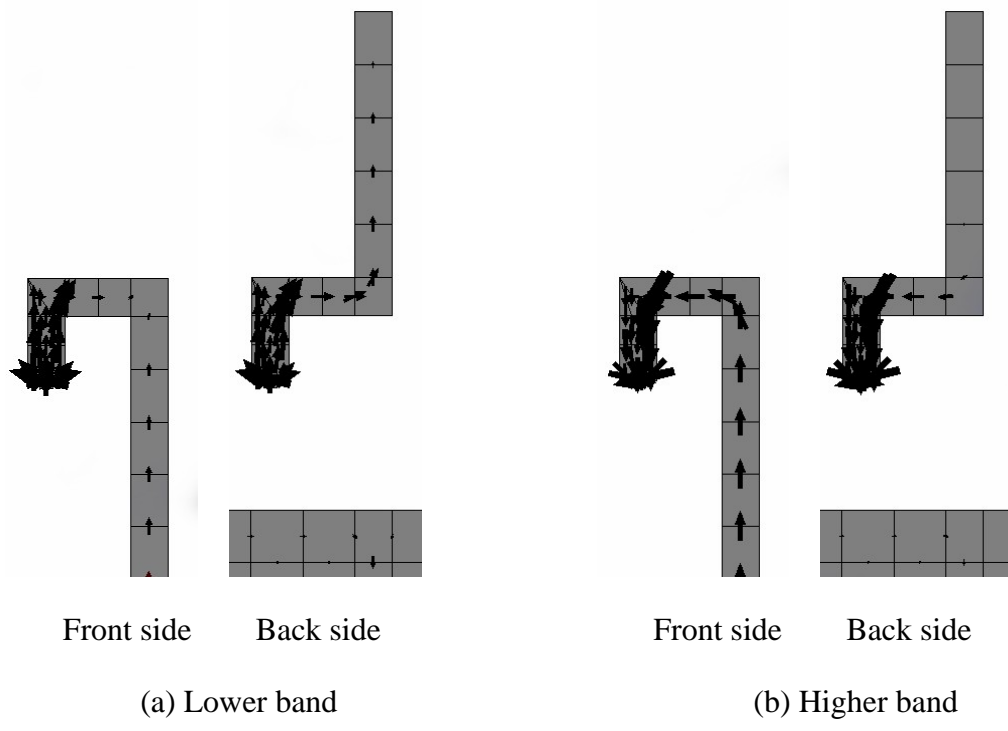


Figure 4-5: Current density distribution of the dual-band antenna

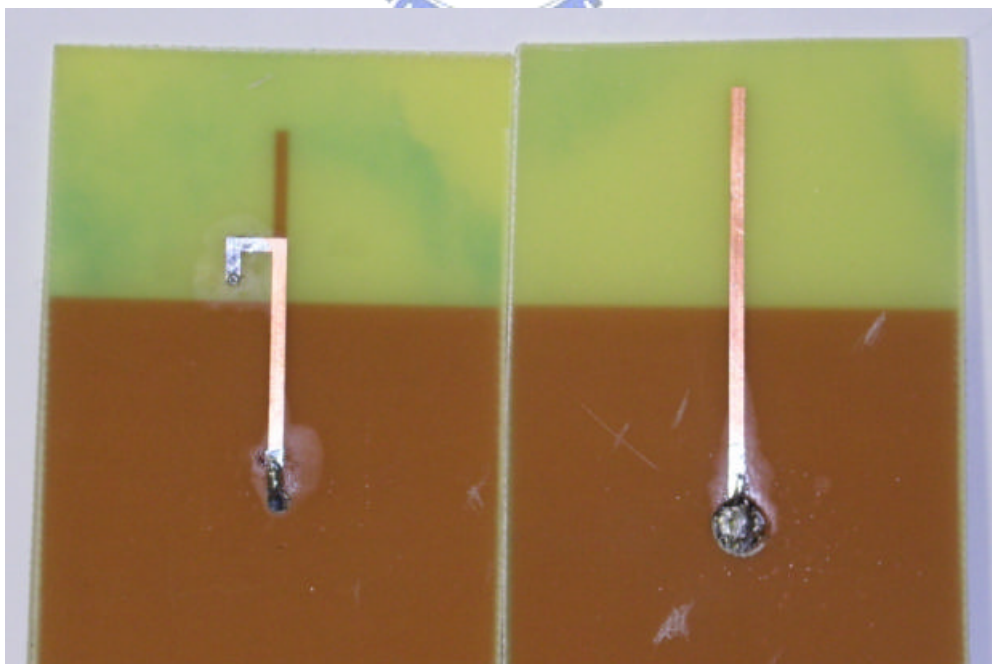
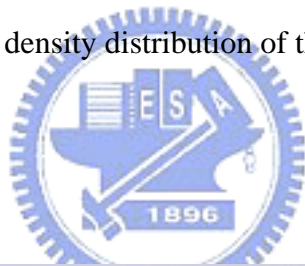


Figure 4-6: Dual-band antenna compared with the typical monopole antenna

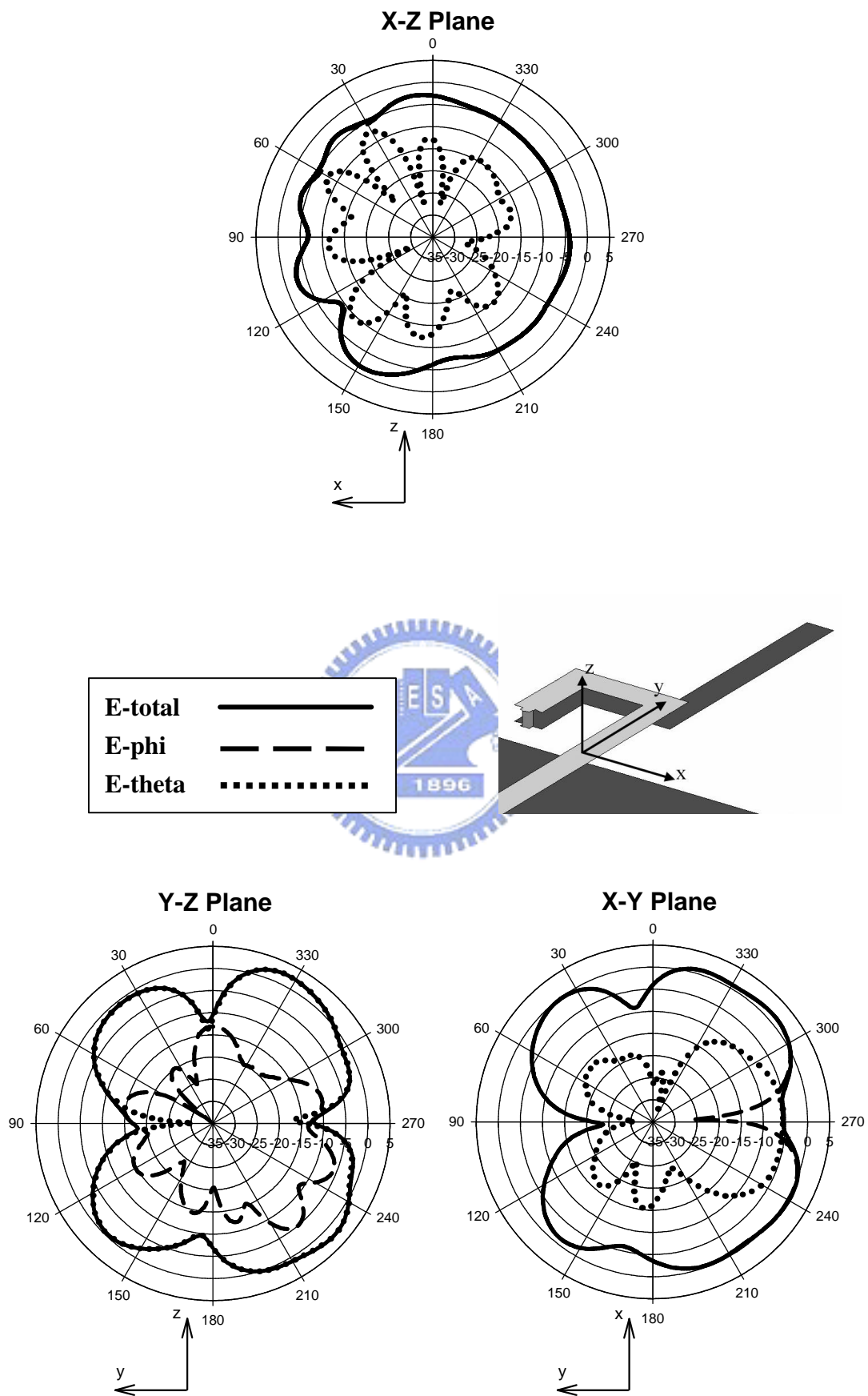


Figure 4-7: Measured radiation patterns of the dual-antenna at 2.44 GHz

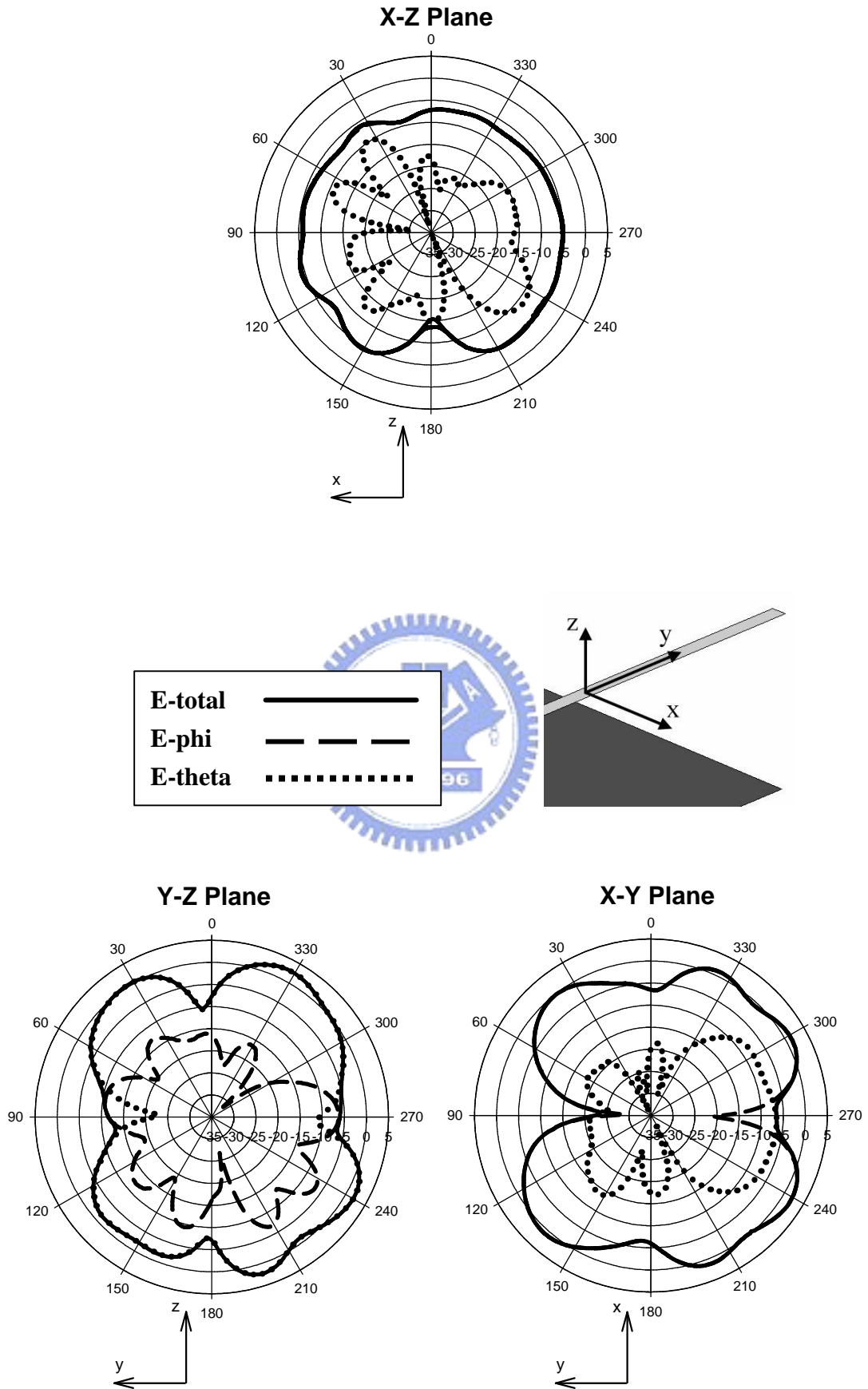


Figure 4-8: Measured radiation patterns of the typical monopole antenna at 2.44 GHz

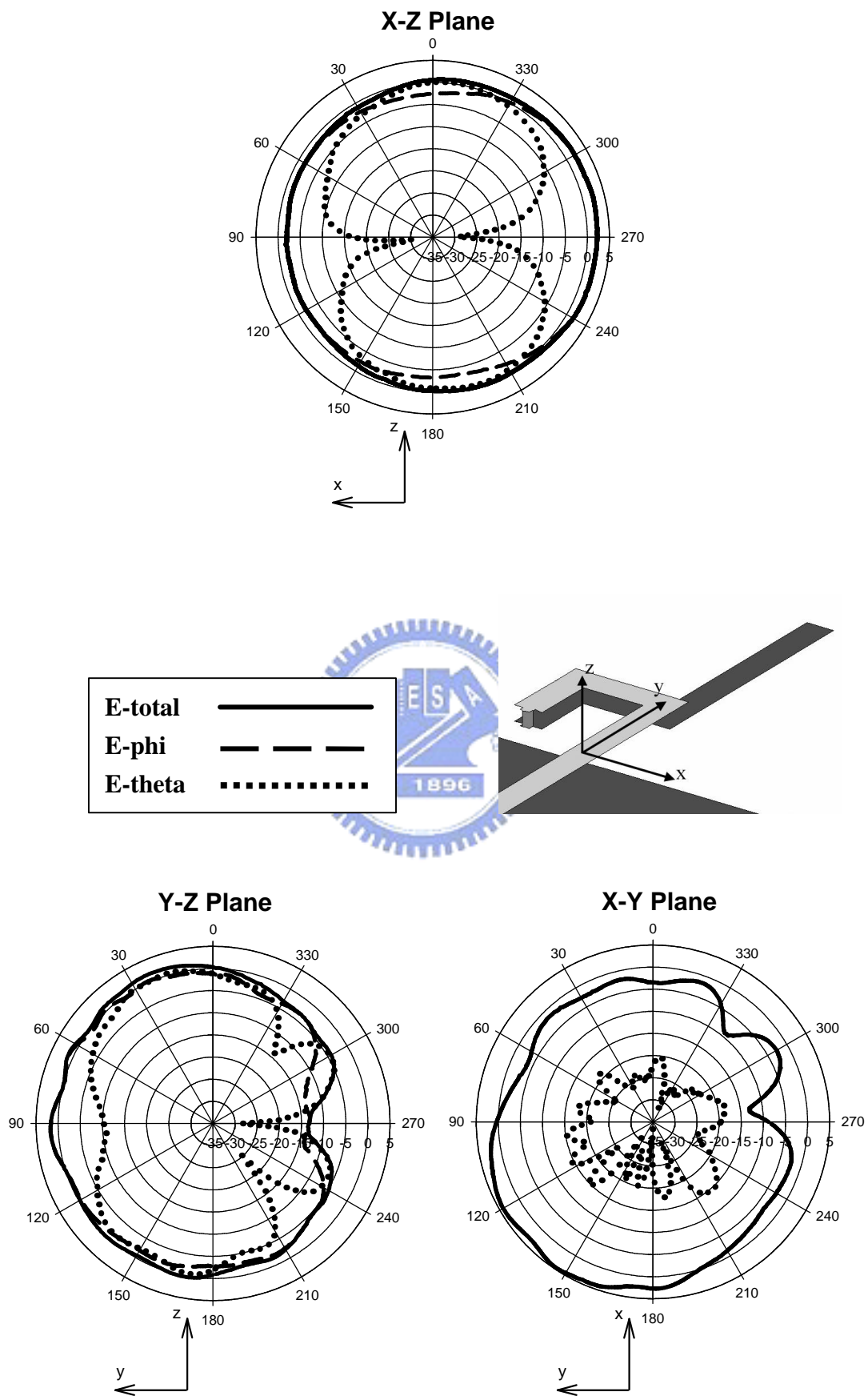


Figure 4-9: Measured radiation patterns of the dual-antenna at 5.25 GHz

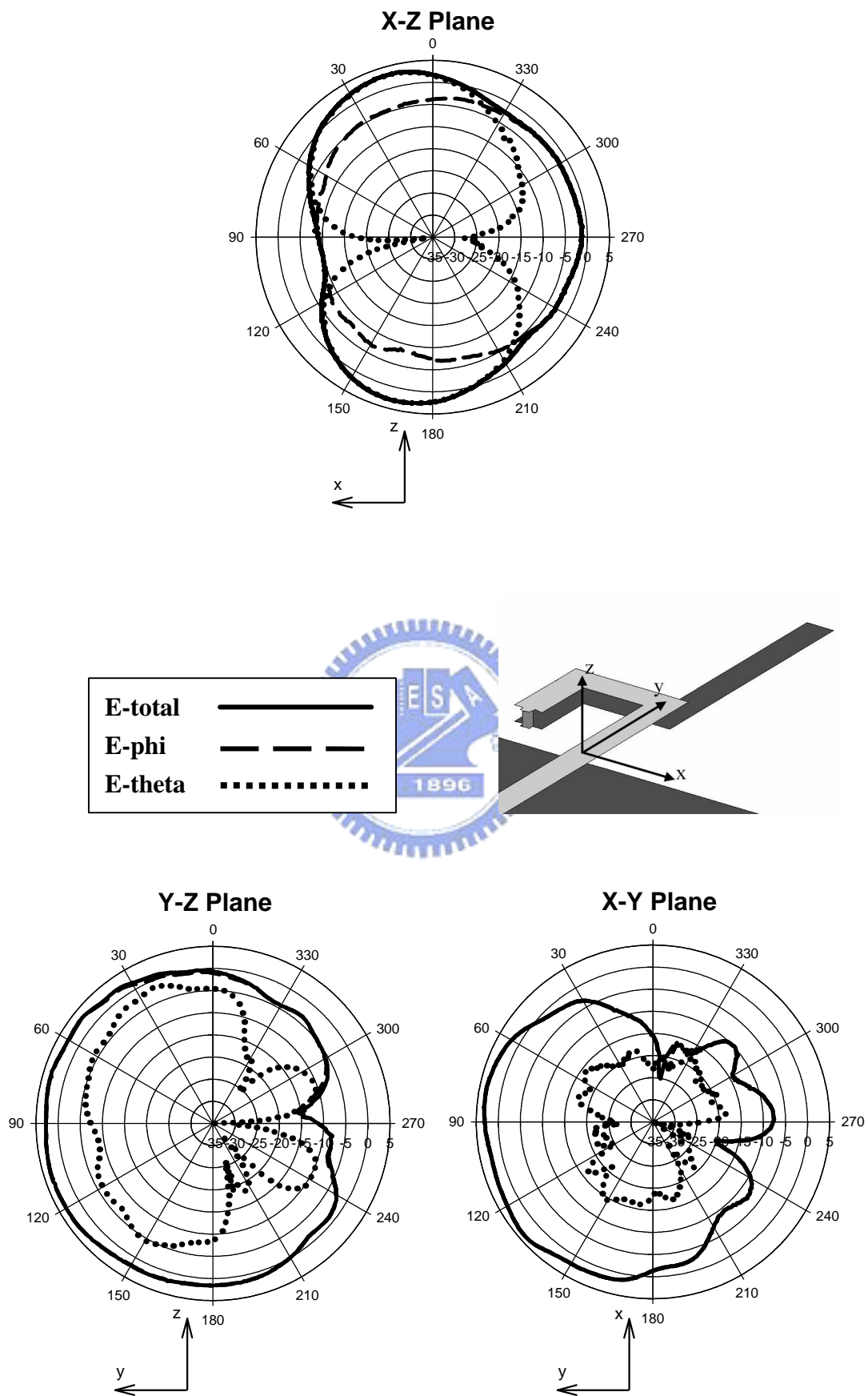
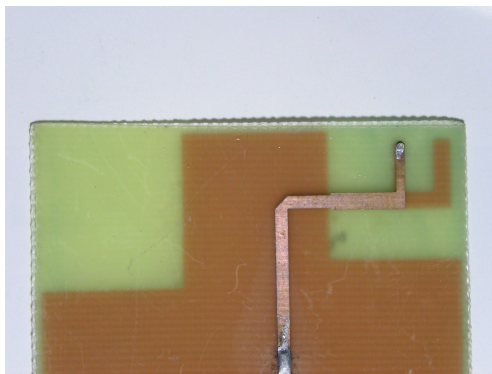
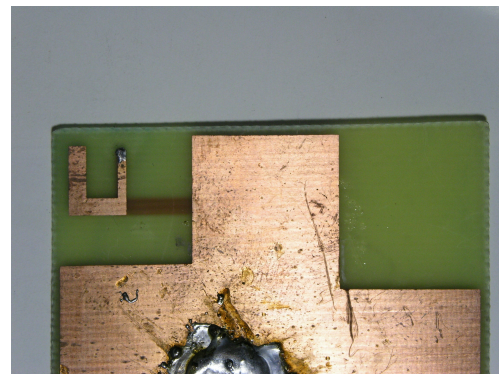


Figure 4-10: Measured radiation patterns of the dual-antenna at 5.77 GHz



(a) Front side



(b) Back side

Figure 4-11: Photography of the modified dual-band antenna

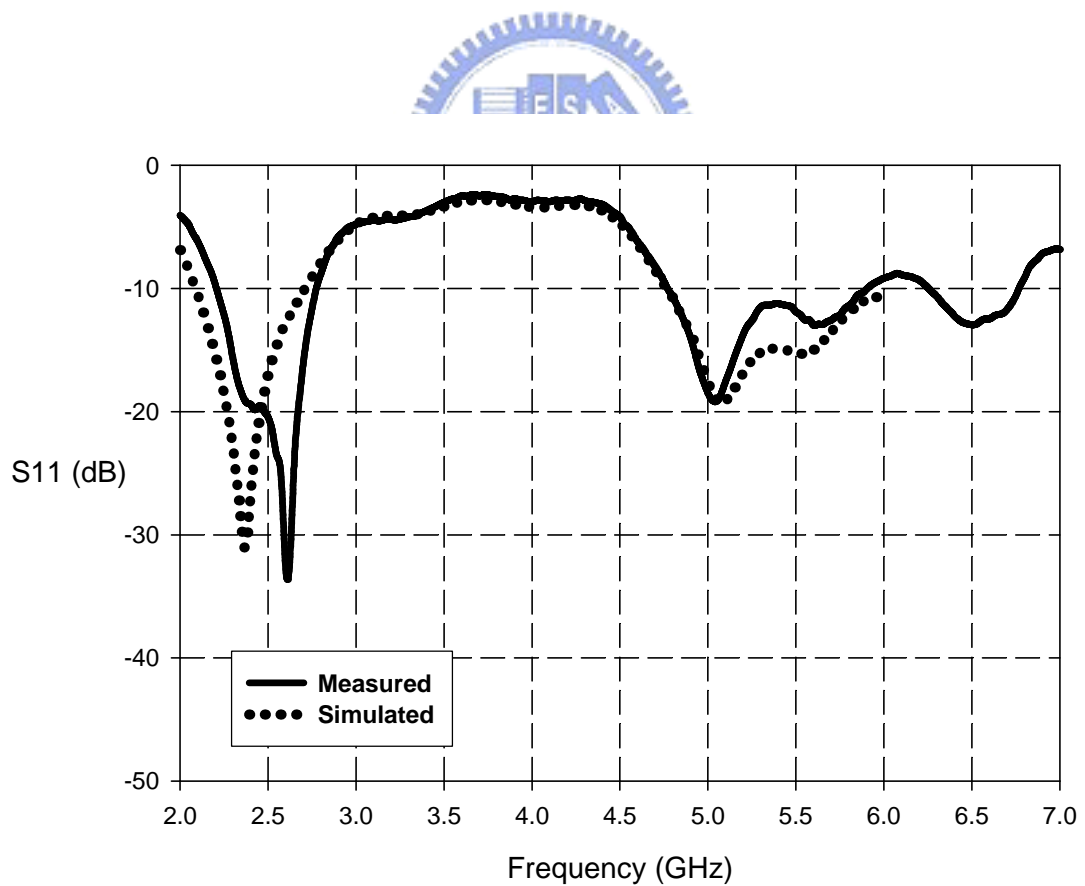


Figure 4-12: Simulated and Measured return loss of the modified dual-band antenna

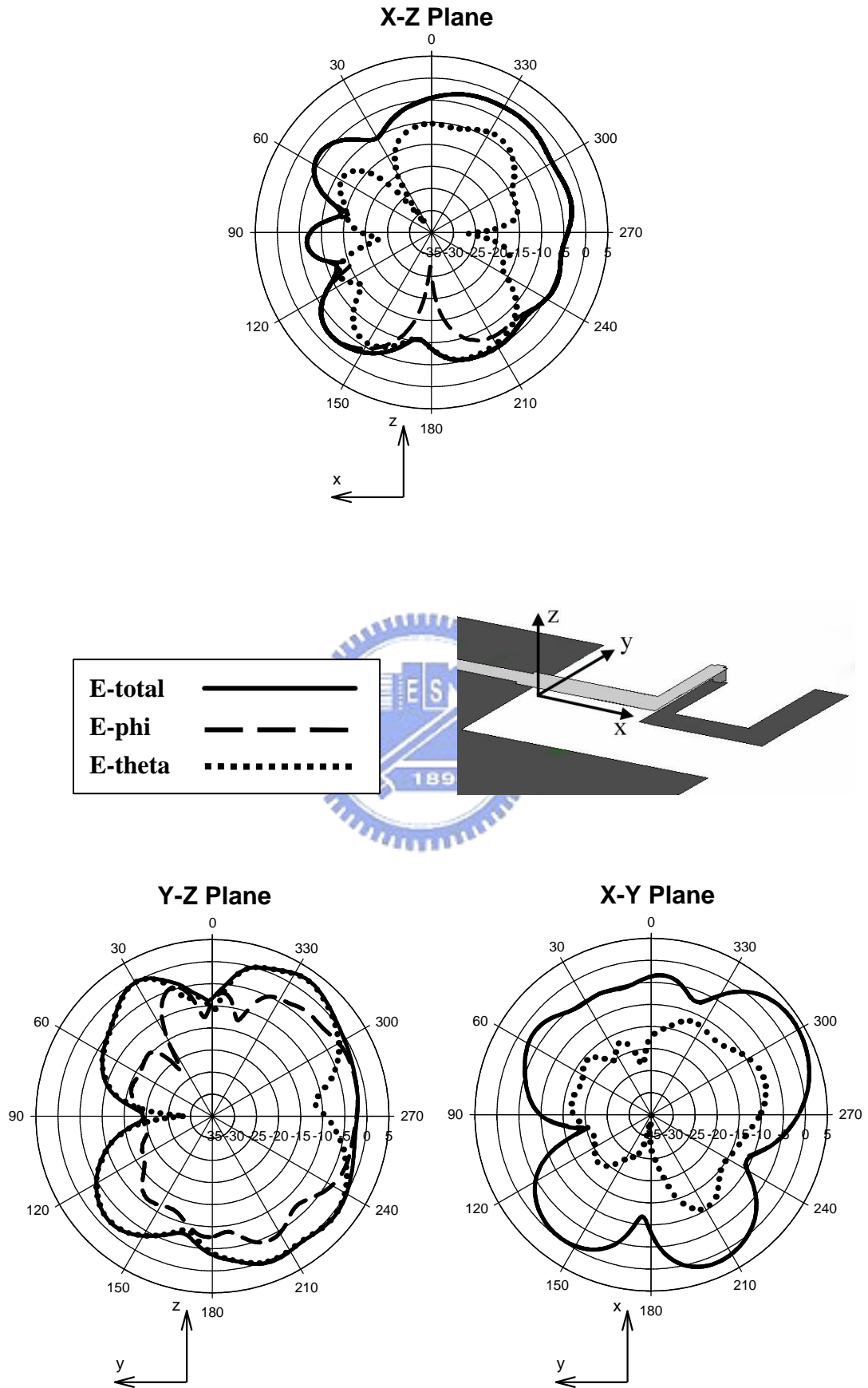


Figure 4-13: Measured radiation patterns of the modified dual-antenna at 2.44 GHz

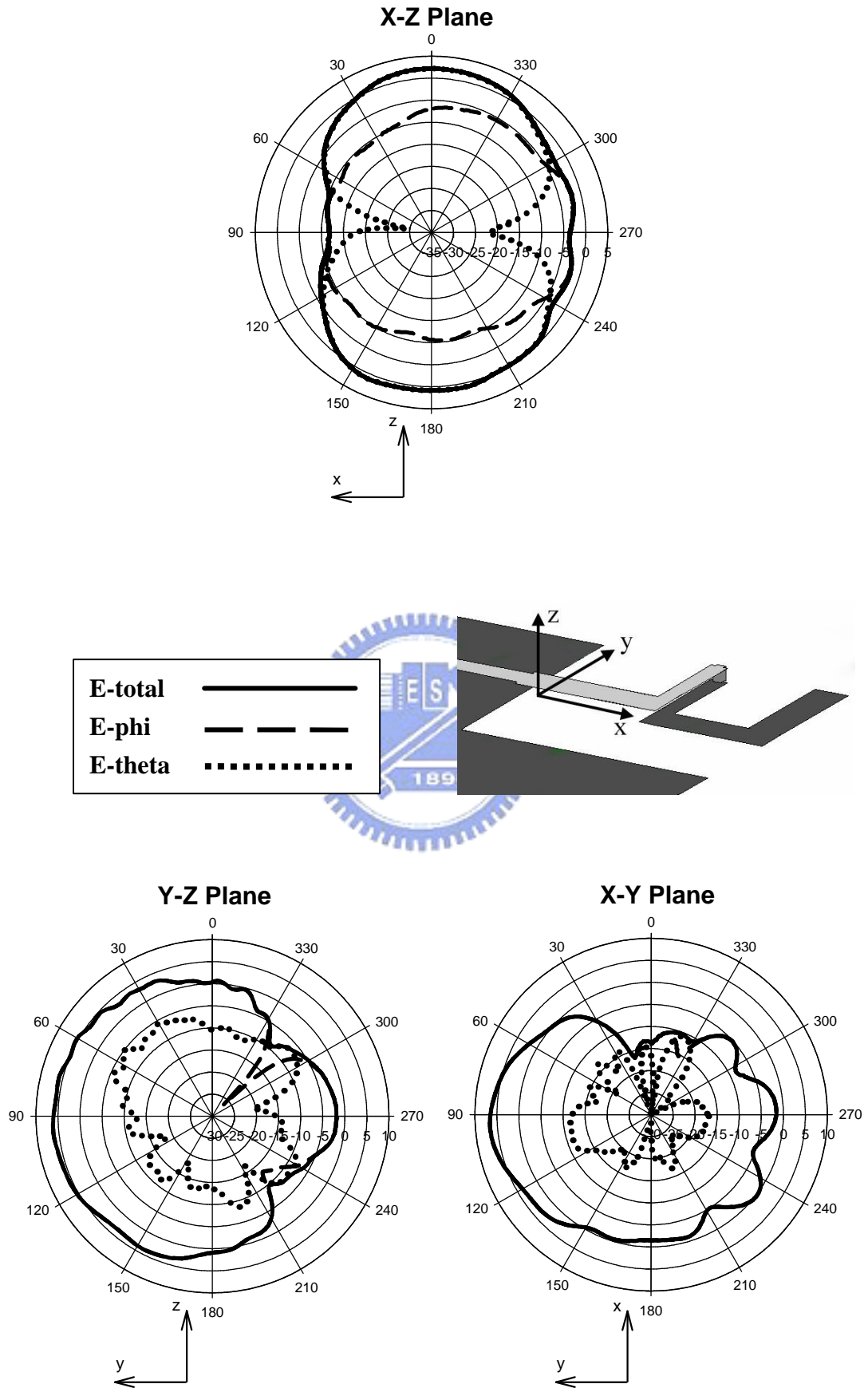


Figure 4-15: Measured radiation patterns of the modified dual-antenna at 5.25 GHz

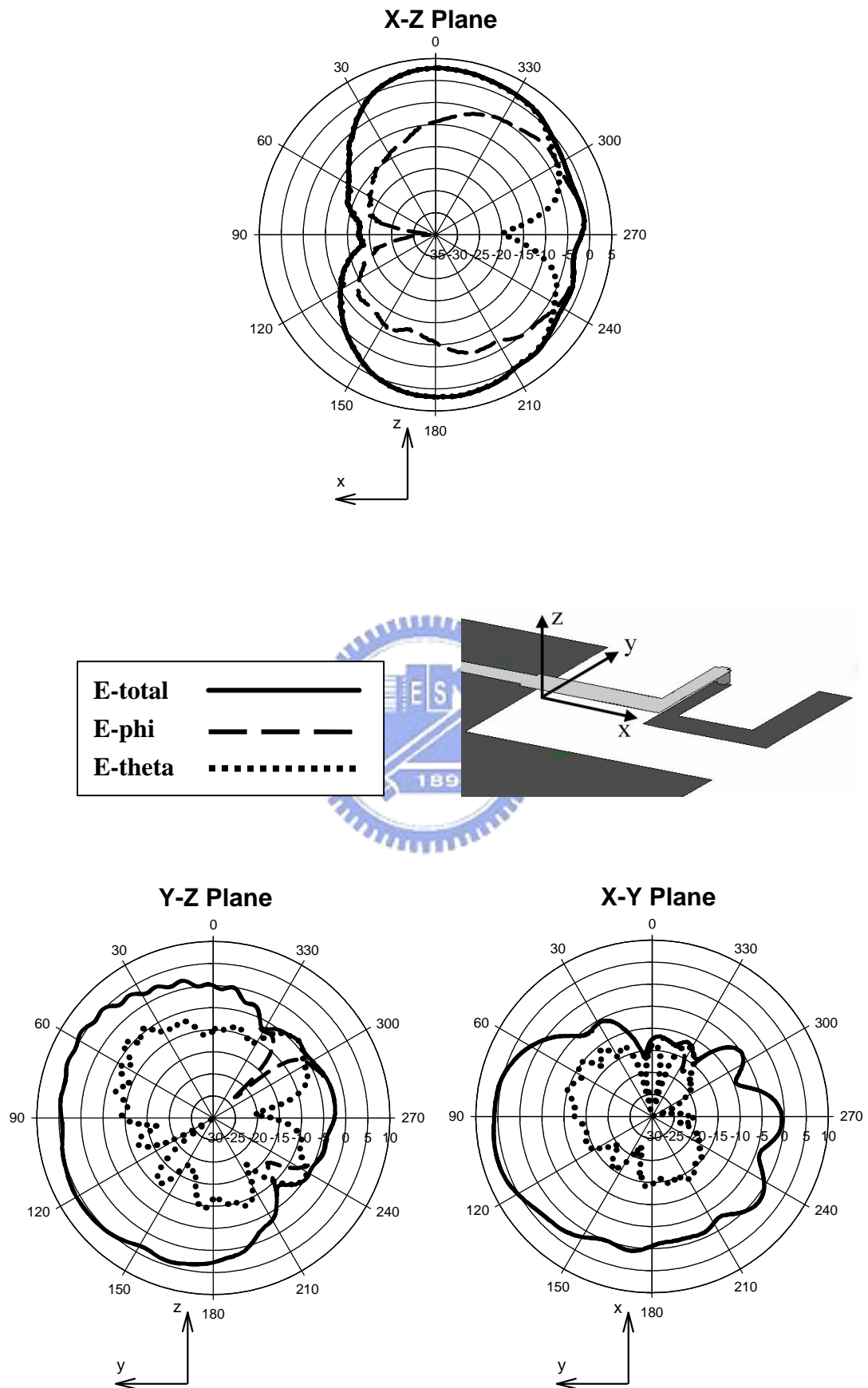


Figure 4-16: Measured radiation patterns of the dual-antenna at 5.77 GHz

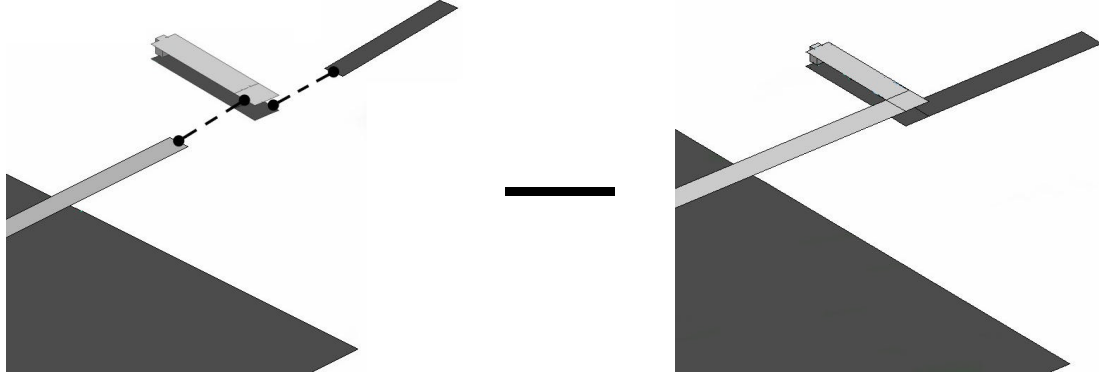


Figure 4-17: Design flow of the dual-band antenna

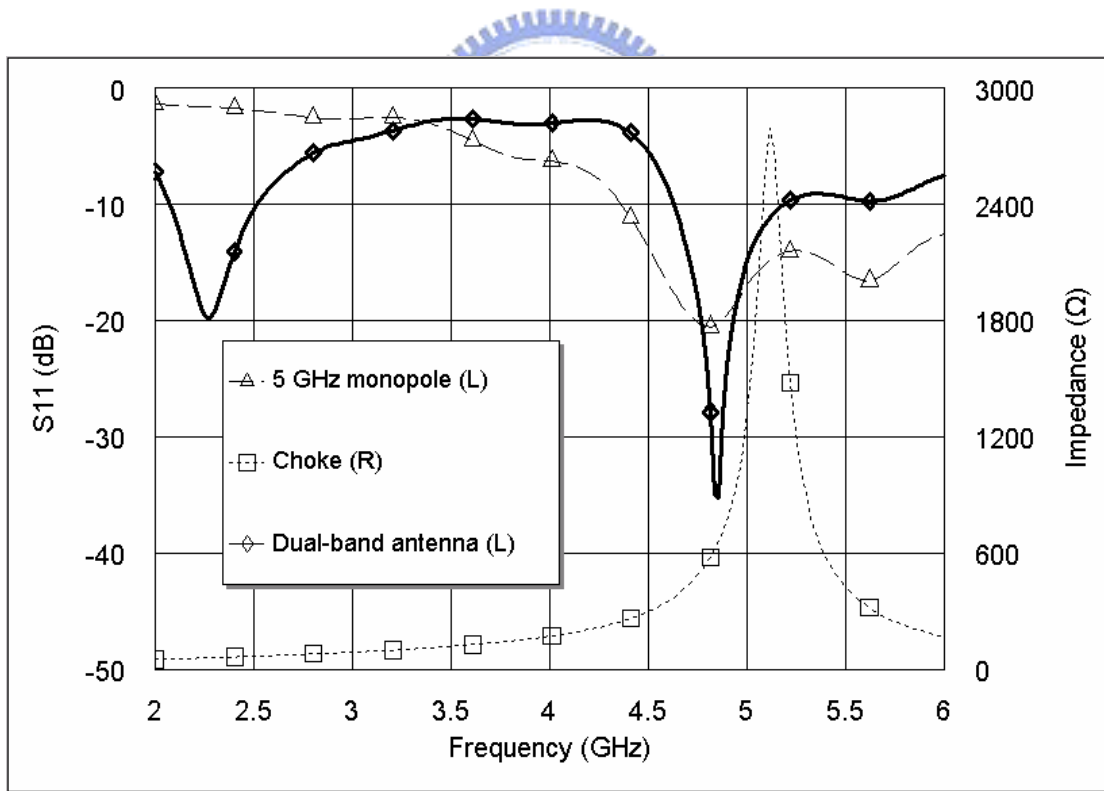


Figure4-18: The result of the dual-band antenna from design flow

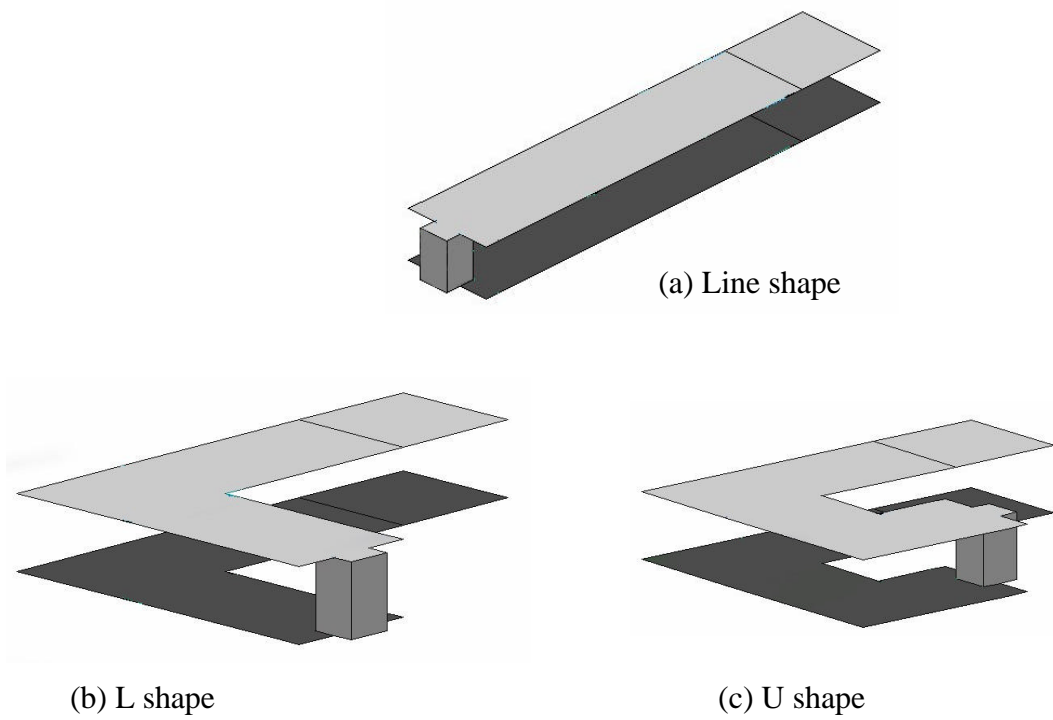


Figure 4-19: Several kinds of the choke shape

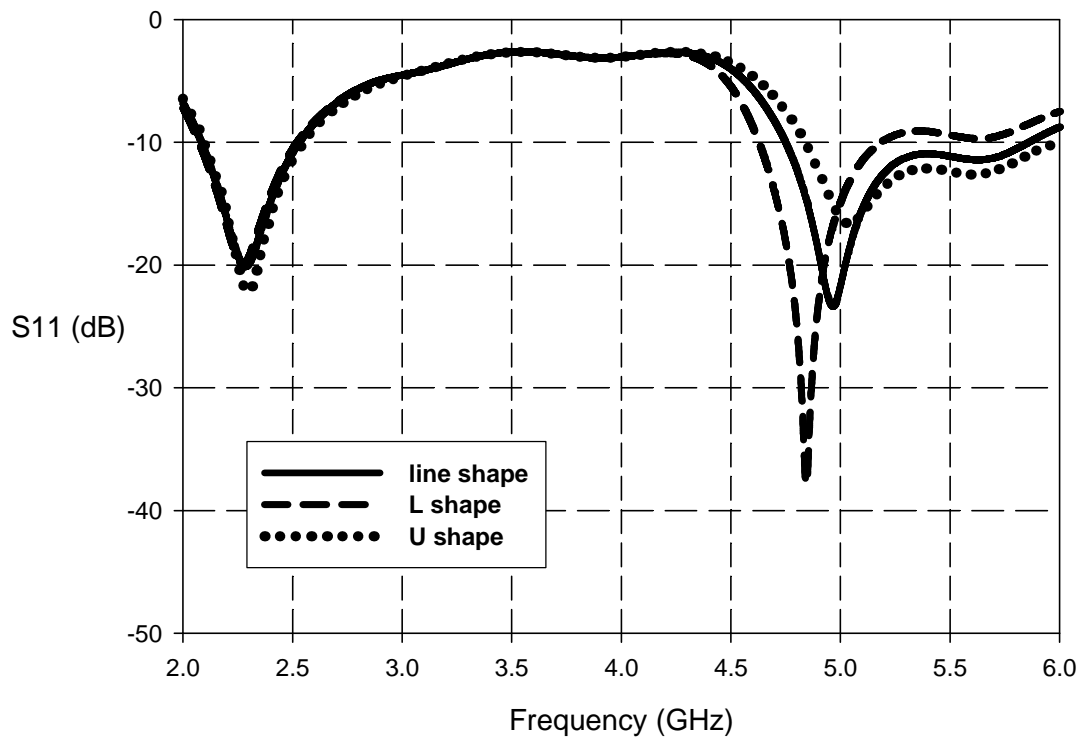


Figure 4-20: Simulated return loss of the dual-band antenna with different choke

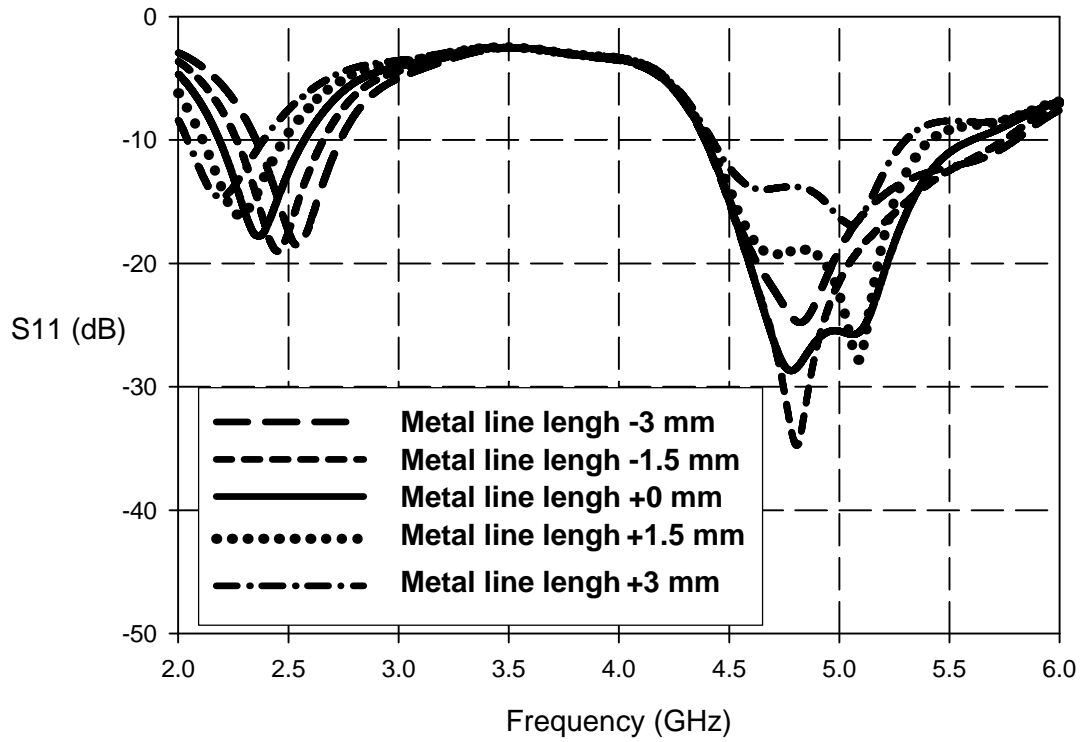


Figure 4-21: Simulated return loss of the dual-band antenna with different tuning metal line length

Chapter 5: Design and Measurement of a Multiple-Band Monopole Antenna with a Microstrip Choke

5.1 Design Theory

We will design a multiple-band antenna for GSM 900/1800/1900 and 802.11 b/g applications. The design idea is similar to the dual-band antenna in the previous chapter. We choose the monopole to resonant at 1.8 or 1.9 GHz and let the choke have infinite impedance at 1.8 GHz or 1.9 GHz. Adding a tuning metal line makes the electrical length from the input of the monopole to the metal line end equals $\lambda/4$ of the 0.9 GHz. Then we add a branch line to the monopole to resonant at 2.4 GHz. There will be a higher order radiation mode of 0.9 GHz in the neighborhood of the 1.8 GHz to 1.9 GHz band. It is important to tune these modes to improve the bandwidth of the 1.8 GHz to 1.9 GHz band.

5.2 Simulated and Measured Results

Figure 5-1 shows the photography of the multiple-band antenna accomplished on a FR4 substrate, whose dielectric constant is 4.7, loss tangent is 0.02, and thickness is 0.8 mm. The feeding line is 50 Ω microstrip line. The EM numerical simulators are Zeland IE3D and Ansoft HFSS. We fabricate the antenna in a $26\text{mm} \times 25\text{mm}$ region surrounding by ground plane. The antenna size is $26\text{mm} \times 17\text{mm}$. The monopole part of the multiple-band antenna is the inverted-L antenna. The choke is a line structure and the tuning metal line is a spiral shape. The branch for 2.4 GHz is a “quasi-hook antenna” structure. Since the antenna is a complex structure and each part is quite

closed to each other, the coupling may induce a higher order radiation mode in the neighborhood of the 1.8 GHz to 1.9 GHz band. Figure 5-2 is the simulated and measured return loss of the multiple-band antenna. It is seen that the multiple-band antenna does exhibit four resonant bands at 0.9 GHz, 1.8 GHz, 1.9 GHz and 2.4 GHz. The 6 dB bandwidth at 0.9 GHz is 80 MHz, which is from 0.875 GHz to 0.955 GHz. The VSWR=2.5 bandwidth at 1.8 GHz and 1.9 GHz is 390 MHz, which is from 1.71 GHz to 2.1 GHz. The 10 dB bandwidth at 2.4 GHz is 350 MHz, which is from 2.36 GHz to 2.61 GHz. Figure 5-3 to Figure 5-6 are the current density distributions of the multiple-band antenna in each band. In Figure 5-3 and Figure 5-5, we can find a dual-band performance because of a microstrip choke. In Figure 5-4, we can find the 1.8 GHz resonant point is the higher order mode of the 0.9 GHz and this resonant point improves the bandwidth of the GSM 1800/1900 band. In Figure 5-6, we can find the branch line is dominant the radiation performance of 2.4 GHz band. Figure 5-7 shows the measured radiation patterns of the multiple-band antenna at 0.92 GHz. The maximum gain and average gain of X-Z, Y-Z and X-Y plane are listed below:

	X-Z plane	Y-Z plane	X-Y plane
Maximum Gain	1.50 dBi	1.70 dBi	-0.63 dBi
Average Gain	-0.57 dBi	-1.08 dBi	-1.91 dBi

Table 5-1: The maximum and average gain of the multiple-band antenna in the X-Z, Y-Z and X-Y plane at 0.92 GHz.

Figure 5-8 shows the measured radiation patterns of the multiple-band antenna at 1.795 GHz. The maximum gain and average gain of X-Z, Y-Z and X-Y plane are listed below:

	X-Z plane	Y-Z plane	X-Y plane
Maximum Gain	-1.43 dBi	0.68 dBi	-0.63 dBi
Average Gain	-1.40 dBi	-1.13 dBi	-1.91 dBi

Table 5-2: The maximum and average gain of the multiple-band antenna in the X-Z, Y-Z and X-Y plane at 1.795 GHz.

Figure 5-9 shows the measured radiation patterns of the multiple-band antenna at 1.92 GHz. The maximum gain and average gain of X-Z, Y-Z and X-Y plane are listed below:

	X-Z plane	Y-Z plane	X-Y plane
Maximum Gain	1.54 dBi	2.66 dBi	2.64 dBi
Average Gain	-0.14 dBi	0.26 dBi	-0.33 dBi

Table 5-3: The maximum and average gain of the multiple-band antenna in the X-Z, Y-Z and X-Y plane at 1.92 GHz.

Figure 5-10 shows the measured radiation patterns of the multiple-band antenna at 2.44 GHz. The maximum gain and average gain of X-Z, Y-Z and X-Y plane are listed below:

	X-Z plane	Y-Z plane	X-Y plane
Maximum Gain	1.18 dBi	1.46 dBi	4.22 dBi
Average Gain	-0.63 dBi	-0.36 dBi	-0.84 dBi

Table 5-4: The maximum and average gain of the multiple-band antenna in the X-Z, Y-Z and X-Y plane at 2.44 GHz.

5.3 Analysis

This multiple-band antenna is similar to the dual-band antenna discussed in Chapter 4. But it is more difficult to design since the wavelength of 0.9 GHz is too long. For 0.9 GHz, this size will perform like a short-dipole antenna and have higher Q-value. So the bandwidth is narrower. It is the most serious problem to overcome. Decreasing the complexity of the antenna structure or a bit magnifying the antenna size will improve the bandwidth of the antenna at 0.9 GHz band. Similar to the dual-band antenna, the design flow shown in Chapter 4 is also suitable for the antenna. Figure 5-11 shows the simulated result of the multiple-band antenna without the 2.4 GHz branch from the design flow. We can find the result has less offset than the 2.4 GHz and 5.2 GHz dual-band antenna discussed in Chapter 4. The result from the design flow is more accurate at lower frequency. If we remove the inverted-L antenna, the choke and the tuning metal line, the branch is like a bent monopole antenna. The dash line in Figure 5-12 is the simulated return loss of the bent monopole antenna. Its resonant frequency is a bit lower than the highest resonant frequency of the multiple-band antenna but it has a broad bandwidth. So the branch can dominant the 2.4 GHz radiation performance. If we add the inverted-L antenna to the bent monopole antenna, the dash-dot line is the simulated return loss. It is a dual-band antenna at 1.9 GHz and 2.4 GHz.

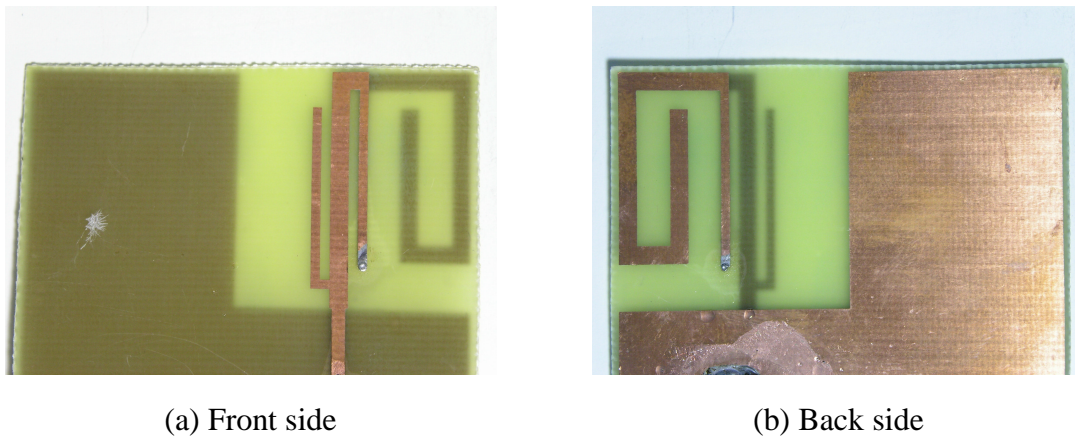


Figure 5-1: Photography of the multiple-band antenna

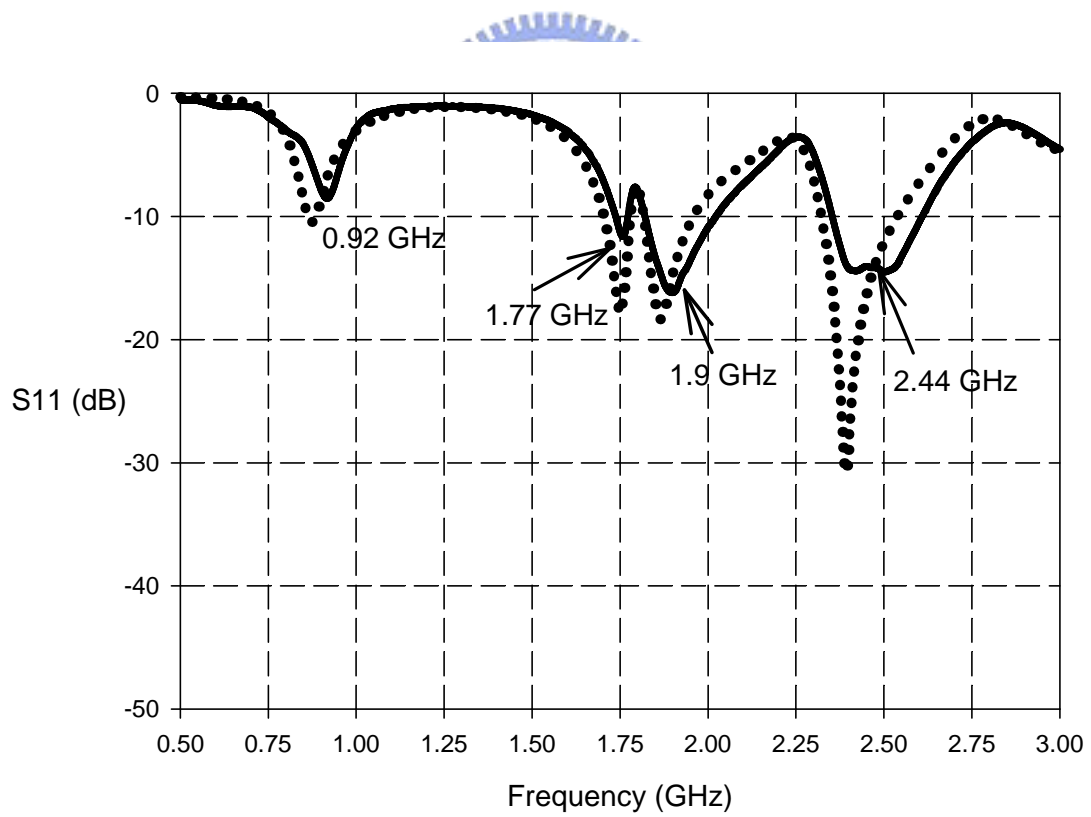
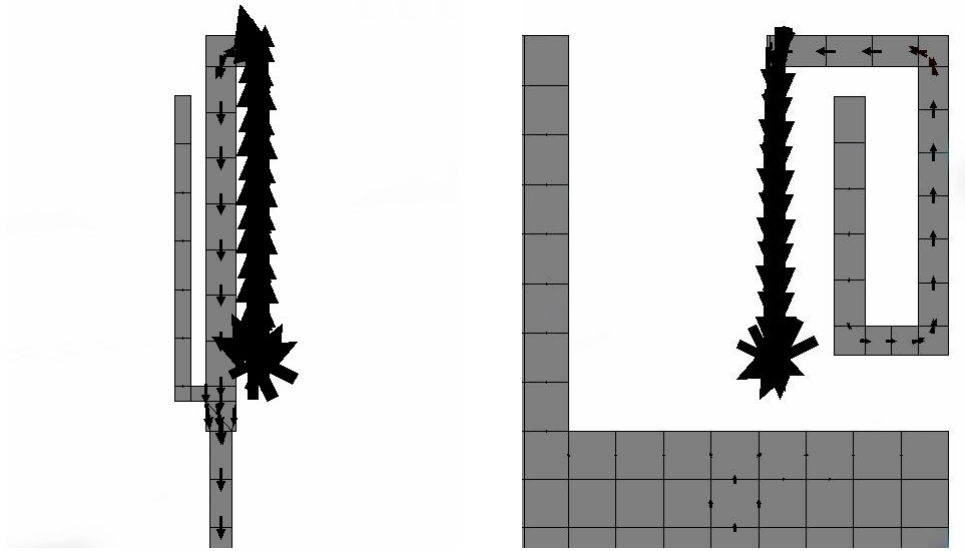


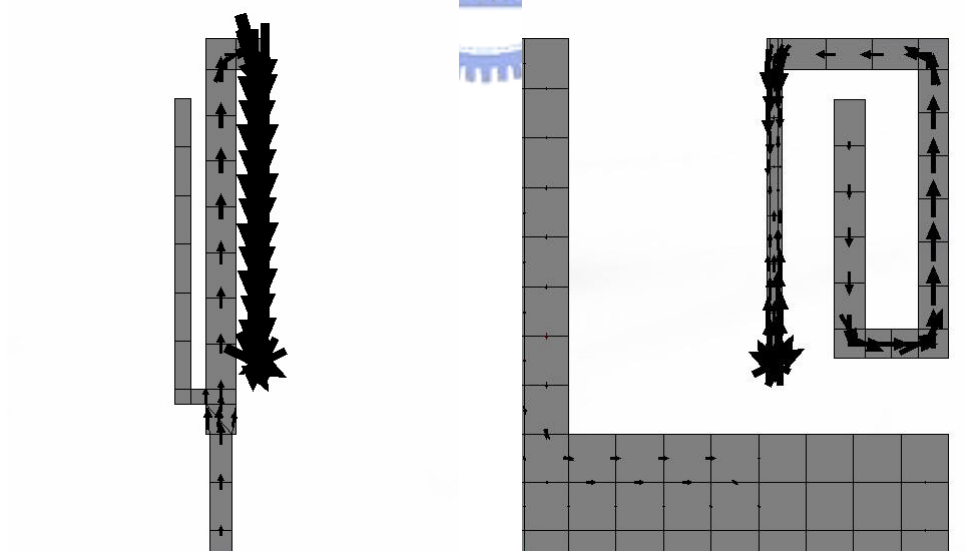
Figure 5-2: Simulated and measured return loss of the multiple-band antenna



(a) Front side

(b) Back side

Figure 5-3: Current distribution of the multiple-band antenna at 0.9 GHz band



(a) Front side

(b) Back side

Figure 5-4: Current distribution of the multiple-band antenna at 1.8 GHz band

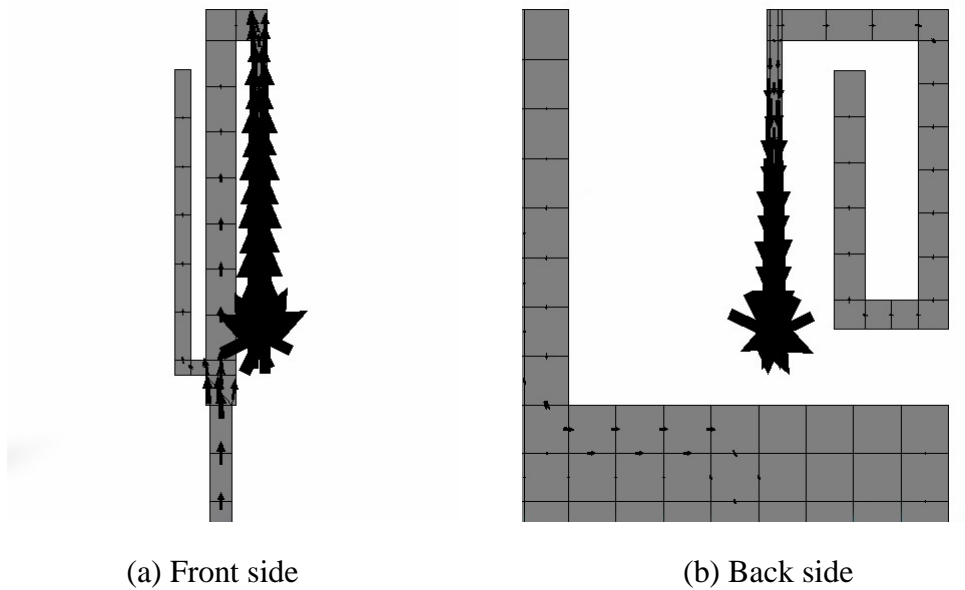


Figure 5-5: Current distribution of the multiple-band antenna at 1.9 GHz band

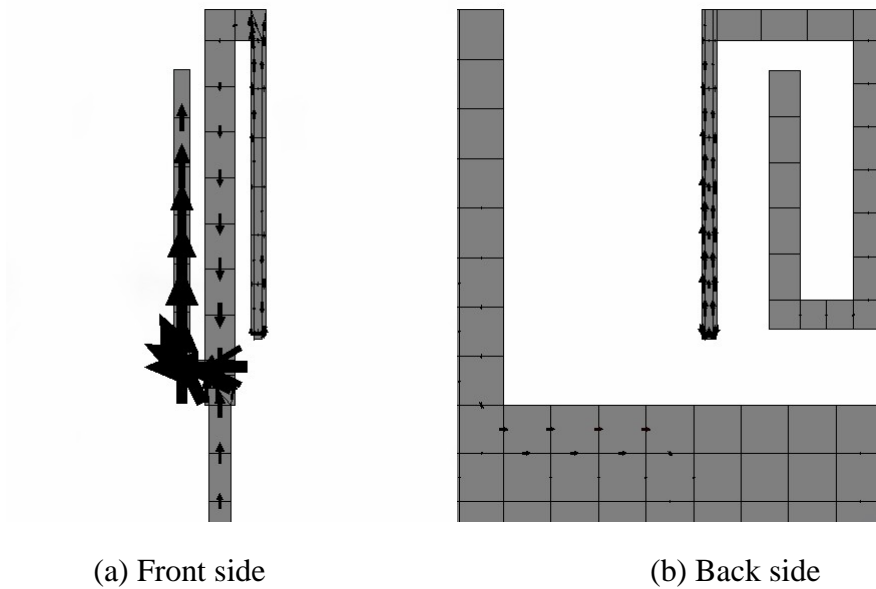


Figure 5-6: Current distribution of the multiple-band antenna at 2.4 GHz band

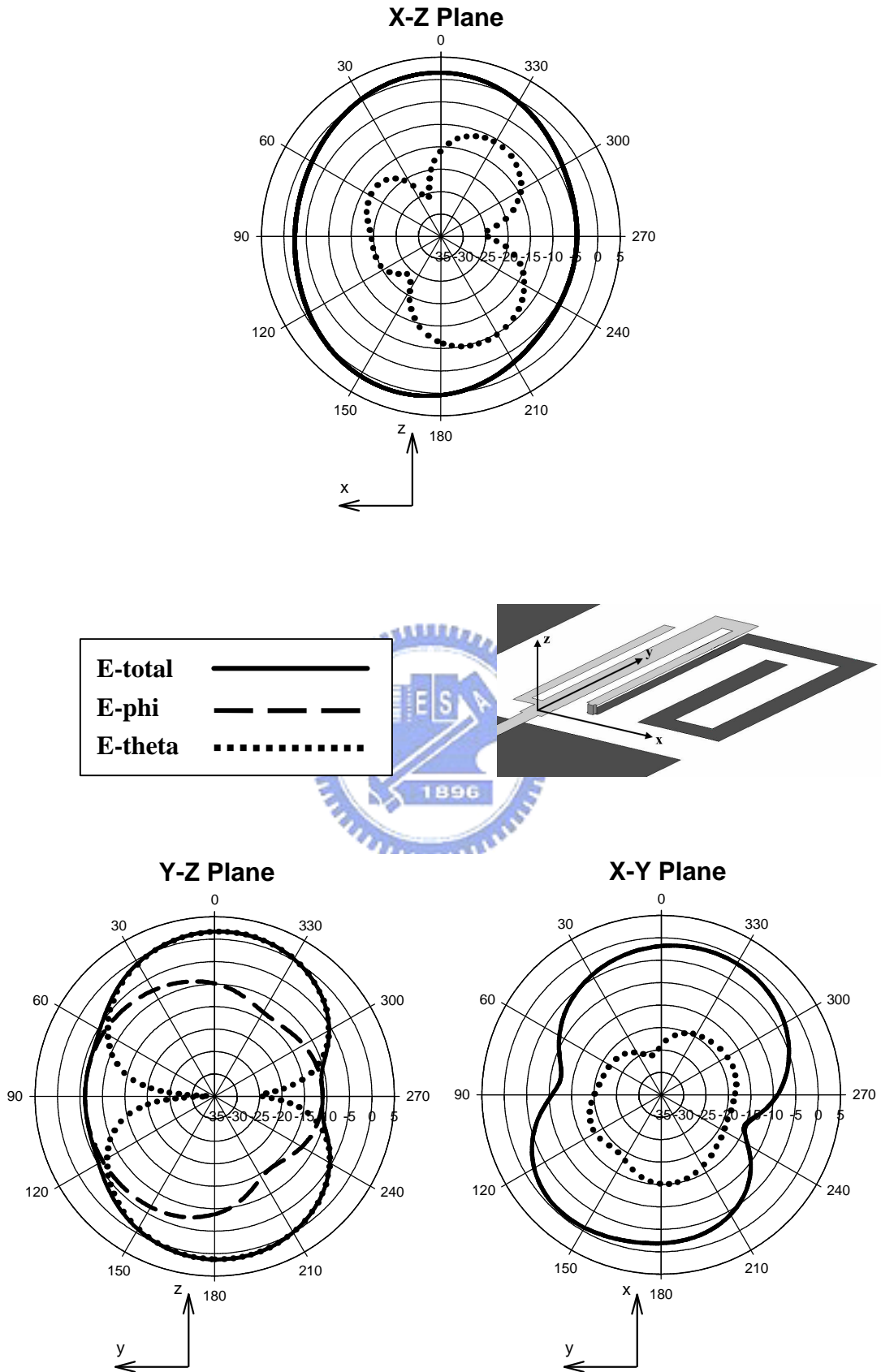


Figure 5-7: Radiation patterns of the multiple-band antenna at 0.92 GHz

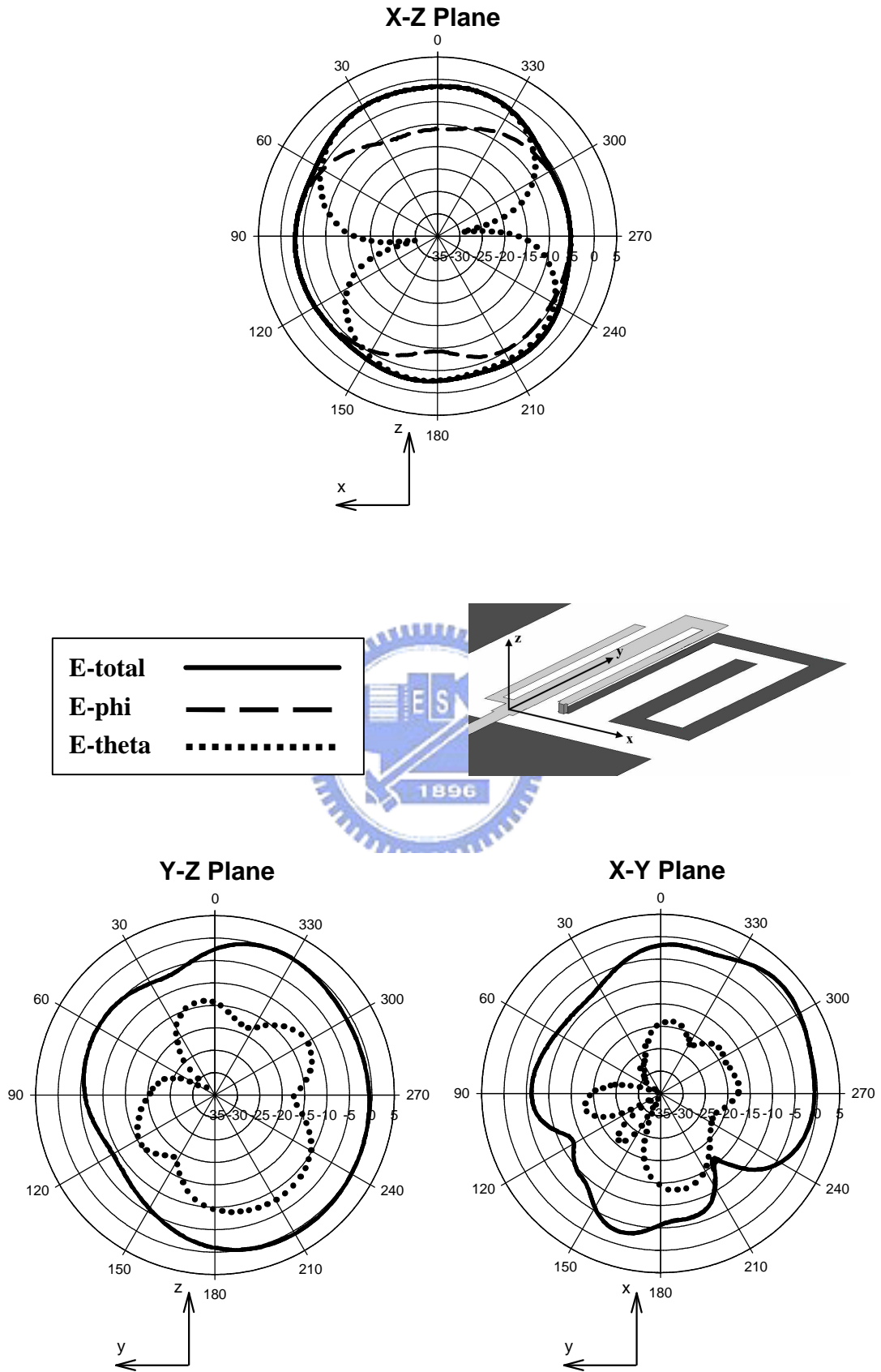


Figure 5-8: Radiation patterns of the multiple-band antenna at 1.795 GHz

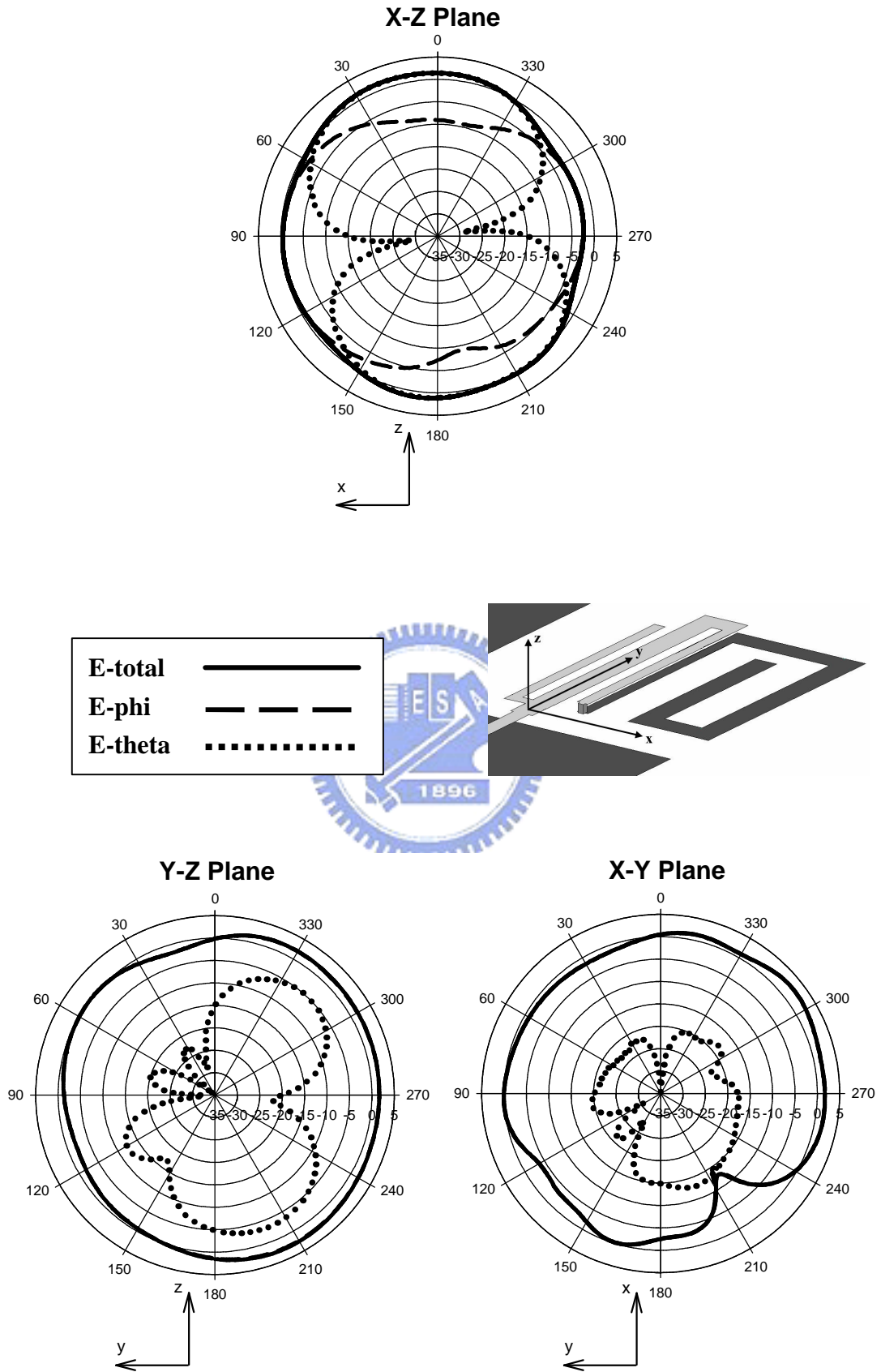


Figure 5-9: Radiation patterns of the multiple-band antenna at 1.92 GHz

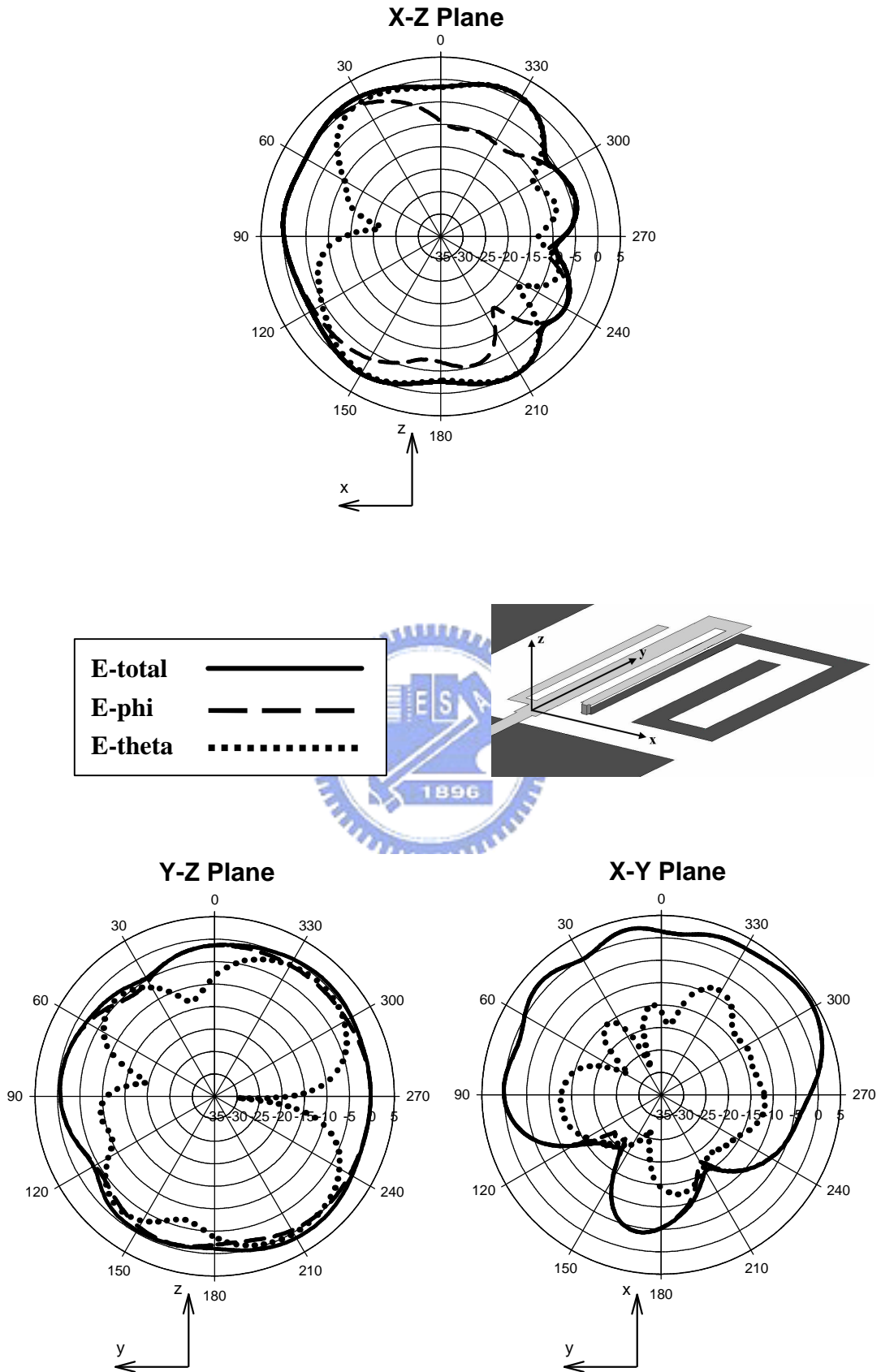


Figure 5-10: Radiation patterns of the multiple-band antenna at 2.44 GHz

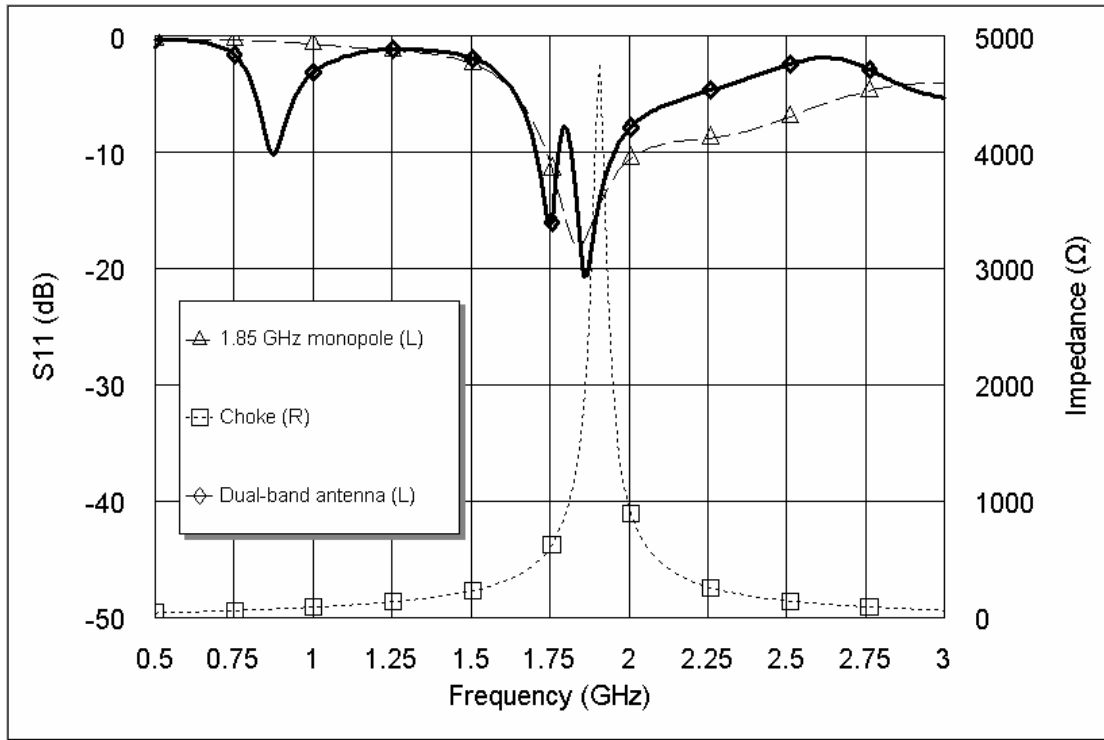


Figure 5-11: Result of the dual-band antenna section from the design flow

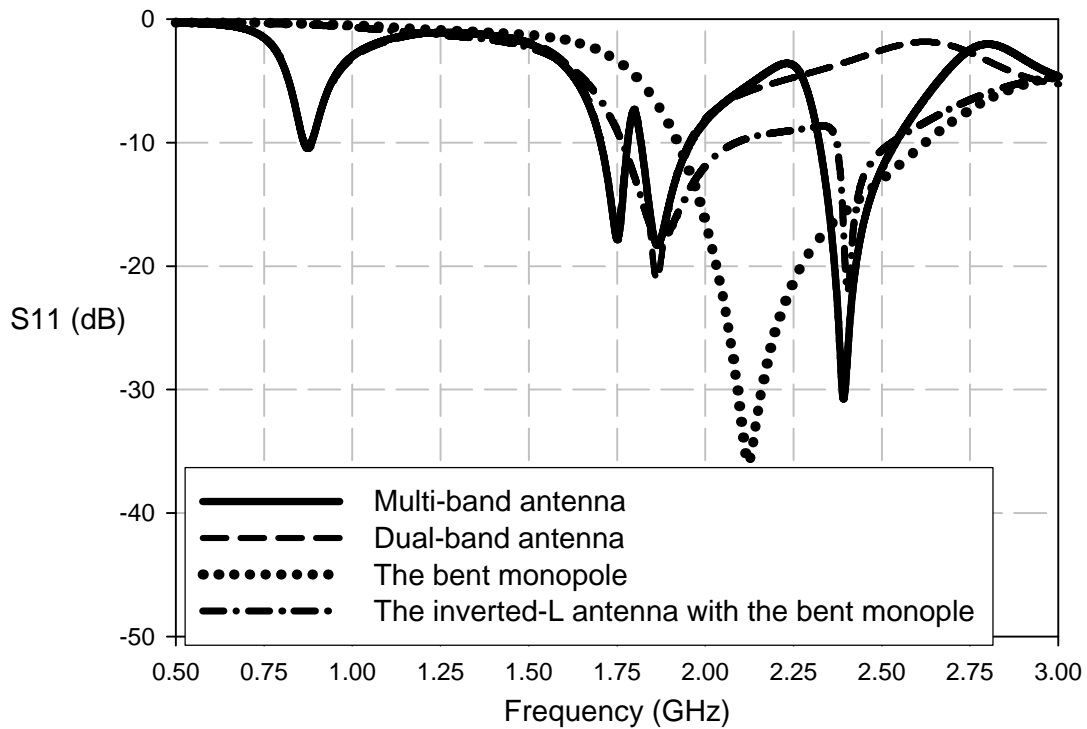


Figure 5-12: Comparison with each section of the multiple-band antenna

Chapter 6: Conclusions

In this thesis, three novel printed antennas fabricated on the FR4 substrate are demonstrated.

The printed inverted-E antenna has been reported in Chapter 3. The bandwidth of this compact antenna is 335 MHz. The printed inverted-E antenna has omni-directional radiation patterns. The maximum gain is 2.08 dBi and average gain of certain plane can reach 0.04 dBi. If we add a protecting case to the antenna, the bandwidth is slightly reduced to 240 MHz. The radiation patterns almost keep omni-directional. The maximum gain is 1.43 dBi and average gain of certain plane can reach -0.51 dBi.

The dual-band antenna utilizing a microstrip choke has been reported in Chapter 4. It is a novel antenna to operate in dual-band. The bandwidth of the dual-band antenna in lower band is 350 MHz and that in higher band is 1.05 GHz. The radiation patterns in lower band are similar to a typical monopole antenna and that in higher band are nearly omni-directional. The maximum gain in the lower band is 2.43 dBi, in the 5.25 GHz band is 4.58 dBi and in the 5.77 GHz band is 3.78 dBi. The average gain of certain plane can reach -1.17 dBi at lower frequency, 0.03 dBi in 5.25 GHz band and -0.07 dBi in 5.77 GHz band. The bent metal line can reduce the size of the antenna. The bandwidth of the modified antenna is 520 MHz in lower band and 1.12 GHz in higher band. The maximum gain in the lower band is 3.59 dBi, in the 5.25 GHz band is 6.6 dBi and in the 5.77 GHz band is 6.39 dBi. The average gain of certain plane can reach -1.17 dBi at lower frequency, 0.44 dBi in 5.25 GHz band, and 0.50 dBi in 5.77 GHz band.

The multiple-band antenna utilizing a microstrip choke has been reported in Chapter 5. It is a novel antenna to operate in multiple-band. The bandwidth of the

multiple-band antenna in 0.9 GHz band is 80 MHz, in 1.8GHz to 1.9GHz band is 390 MHz and in 2.4 GHz band is 350MHz. The maximum gain in the lowest band is 1.70 dBi, in the 1.8 GHz band is 0.68 dBi, in the 1.9 GHz band is 2.66 dBi and in the 2.4 GHz band is 4.22 dBi. The average gain of certain plane can reach -1.08 dBi in 0.9 GHz band, -1.13 dBi in 1.8 GHz band, 0.26 dBi in 1.9 GHz band and -0.36 dBi in 2.4 GHz band.

The design of antennas is an art of elaboration. Several recommendations for the design of antennas are dedicated in the following:

- 1) The simulated and measured results in return loss may have some frequency offsets. But the errors are nearly the same for each experiment. The designers should use the magnitude of the errors to calibrate the offsets between the simulated and measured results so that they can achieve the measured results in expected band.
- 2) The simulated radiation patterns using HFSS, instead of IE3D, have extremely correspondence to the measured ones.
- 3) The fabrication of the via-holes on the antennas has enormous influence on the impedance matching of the antennas. The solder on the via-holes must be flatted to the metal.

These recommendations are extremely valuable for the design of antennas. The author hopes that the antennas designers should adopt these as the best regards.

Reference

- [1] Eric V. Stewart, “No Information Security Department? No Problem! A Practical Guide to Securing Wireless Networks”, GSEC Practical Assignment v. 1.4b, Aug. 29 2002
- [2] Katsibas, K.D.; Balanis, C.A.; Tirkas, P.A.; Birtcher, C.R., “Print loop antennas for mobile communications”, Electronics, Circuits, and Systems, 1996, ICECS '96., Proceedings of the Third IEEE International Conference on, Volume: 1, 13-16 Oct. 1996 Pages: 307 - 310 vol.1
- [3] Zi Dong Liu; Hall, P.S.; Wake, D., “Dual-frequency planar inverted-F antenna”, Antennas and Propagation, IEEE Transactions on, Volume: 45, Issue: 10, Oct. 1997 Pages: 1451 – 1458
- [4] Kin-Lu Wong; Gwo-Yun Lee; Tzung-Wern Chiou, “A low-profile planar monopole antenna for multiband operation of mobile handsets”, Antennas and Propagation, IEEE Transactions on, Volume: 51, Issue: 1, Jan. 2003 Pages: 121 - 125
- [5] Horng-Dean Chen; Wen-Shyang Chen; Yuan-Tung Cheng; Yin-Chang Lin, “Dual-band meander monopole antenna”, Antennas and Propagation Society International Symposium, 2003. IEEE, Volume: 3, 22-27 June 2003 Pages: 48 - 51 vol.3
- [6] Pey-Ling Teng; Shyh-Tirng Fang; Kin-Lu Wong, “PIFA with a bent, meandered radiating arm for GSM/DCS dual-band operation”, Antennas and Propagation Society International Symposium, 2003. IEEE, Volume: 3, 22-27 June 2003 Pages: 107 - 110 vol.3
- [7] Shih-Huang Yeh; Kin-Lu Wong; Tzung-Wern Chiou; Shyh-Tirng Fang, “Dual-band planar inverted F antenna for GSM/DCS mobile phones”, Antennas

and Propagation, IEEE Transactions on, Volume: 51, Issue: 5, May 2003
Pages:1124 - 1126

- [8] J. Michael Johnson, Yahya Rahmat-Samii, “The Tab Monopole”, IEEE Transactions on Antennas and Propagation, VOL.45, NO. 1, January 1997 Page(s): 187 -188
- [9] J. Michael Johnson and Yahya Rahmat-Samii, “Wideband Tab Monopole Antenna Array for Wireless Adaptive and Mobile Information Systems Application”, Antennas and Propagation Society International Symposium, 1996. AP-S. Digest On page(s): 718 - 721 vol.1 21-26 July 1996
- [10] Hua-Ming Chen; Yi-Fang Lin; Chin-Chun Kuo; Kuang-Chih Huang, “A compact dual-band microstrip-fed monopole antenna”, Antennas and Propagation Society, 2001 IEEE International Sym , Volume: 2 , 2001 Page(s): 124 -127 vol.2
- [11] H.-M. Chen, “Microstrip-fed dual-frequency printed triangular monopole”, Electronics Letters, Volume: 38 Issue: 13 , 20 June 2002 Page(s): 619 -620
- [12] Yi-Fang Lin; Hua-Ming Chen; Chin-Chun Kuo; Kuang-Chih Huang, “Dual frequency coplanar triangular monopole antenna”, Antennas and Propagation Society International Symposium, 2002. IEEE , Volume: 2 , 2002 Page(s): 48 -51
- [13] Shih-Huang Yeh; Kin-Lu Wong, “Dual-band f-shaped monopole antenna for 2.4/5.2 GHz WLAN application”, Antennas and Propagation Society International Symposium, 2002 IEEE, Volume: 4, 2002 Page(s): 72 -75
- [14] Hao-Chun Tung; Wen-Shyang Chen; Kin-Lu Wong, “Integrated rectangular spiral monopole antenna for 2.4/5.2 GHz dual-band operation”, Antennas and Propagation Society International Symposium, 2002 IEEE, Volume: 3, 2002 Page(s): 496 -499
- [15] W. L. Stutzman; G. A. Thiele, “Antenna theory and design”, 2nd edition, John Wiley & Sons, INC., 1998, Chapter 2, Chapter 5

- [16] F. Cardiol, "Microstrip Circuits", John Wiley & Sons, INC., 1994, Chapter 3
- [17] D. M. Pozar, "Microwave Engineering" John Wiley & Sons, INC., 1998, Chapter 2, Chapter 6
- [18] Rowell, C.R.; "A capacitively loaded PIFA for compact mobile telephone handsets", R.D.; Antennas and Propagation, IEEE Transactions on , Volume: 45 , Issue: 5 , May 1997 Pages:837 - 842

